Research Article
Open Access

MJ Cell Press

MJ Mathematics and Computer Science

Available at:

https://mjcellpress.com/article/mjmcs01/

MJ - MATHEMATICS AND COMPUTER SCIENCE

Mathematical modeling of the Cholera epidemic in Cameroon: From classical-order derivative to fractional-order derivative

Rubin Fandio[1], **Hamadjam Abboubakar**[1,2,3,4*], **Sylvain Ardo Gouroudja Banbeto**[3], **Henri Paul Ekobena Fouda**[1].

[1] *The University of Yaoundé 1, Faculty of Science, Department of Physics, P.O. Box 812 Yaoundé, Cameroon*

[2] *The University of Ngaoundere, University Institute of Technology, Department of Computer Engineering, P.O. Box 455 Ngaoundéré, Cameroon.*

[3] *The University of Ngaoundere, LASE-lab, P.O. Box 112 Ngaoundéré, Cameroon.*

[4] *The University of Ngaoundere, School of Geology and Mining Engineering, Department of Applied Mathematics and Computer Science, P.O. Box 112 Meiganga, Cameroon.*

**Corresponding author: h.abboubakar@gmail.com*

Key words	Abstract
Cholera, Caputo operator, Stability analysis, Calibration and Forecasting, Adam-Bashforth-Moulton, Numerical simulations.	Cholera is a diarrheal disease that was declared a pandemic in 2010, highlighting its reemergence. Southeast Asia and Africa remain at the greatest risk of widespread transmission. The purpose of this study is to develop and analyze a cholera model that incorporates both integer- and fractional-order derivatives in the Caputo sense. After formulating the model, we demonstrate the existence and uniqueness of its solution. We then identify the cholera-free equilibrium point and establish its local and global asymptotic stability whenever the epidemiological threshold $\mathcal{R}_c$ is less than one ($\mathcal{R}_c < 1$). Using real data, we calibrate the model through parameter estimation and forecasting. With the estimated parameters, we observe that $\mathcal{R}c \approx 2.0439$ for the fractional-order parameter $\chi = 1$, and $\mathcal{R}c \approx 1.1121$ for $\chi = 0.90$. To determine which model (classical or fractional) better describes the behavior of the disease, we compute the Root Mean Square Error (RMSE) for each case and find $RMSE_{\xi=1} = 67789.02 > RMSE_{\xi=0.90} = 67767.54$. This demonstrates that the fractional-order cholera model is more suitable for predicting the disease dynamics. Finally, to simulate our fractional model, we employ the Adams–Bashforth–Moulton approach and run numerical simulations to confirm our theoretical conclusions.

Received: 16.02.2025 Accepted: 26.05.2025 Published online: 07.09.2025

How to cite this article: Fandio, R., Abboubakar, H., Banbeto, S. A. G., & Fouda, H. P. E. (2025). *Mathematical modeling of the Cholera epidemic in Cameroon: From classical-order derivative to fractional-order derivative.* **MJ Mathematics and Computer Science, 1**(1), 1–32. https://doi.org/10.63156/mjmcs01.

1 Introduction

Cholera is a global public health problem and a marker of inequality and inadequate socioeconomic development. It is caused by the bacterium *Vibrio cholerae* [1]. Consumption of food or water contaminated with this bacillus leads to an acute diarrheal infection that can cause severe dehydration and kidney failure. Cholera spreads either directly between humans through the fecal–oral route or indirectly through the ingestion of contaminated water and food. The World Health Organization (WHO) warns that untreated infection can lead to death within 12 to 48 hours [2, 3]. Each year, cholera is responsible for an estimated 1.3 to 4.0 million infections in endemic areas and between 21,000 and 143,000 deaths worldwide [4]. As a pandemic disease, cholera continues to reemerge due to its short incubation period, the rapid increase in patient numbers, and its potential for explosive outbreaks. Southeast Asia and Africa are at greatest risk, with high mortality rates exacerbated by insufficient treatment facilities [5]. Historically, the first recorded outbreak occurred in India in 1817 [6, 7], while Yemen has recently experienced the largest cholera outbreak in history [8].

In Cameroon, an epidemic occurred between October 7, 2021, and March 10, 2022, with nearly 10,000 reported cases. According to Report No. 12 on cholera management in Cameroon for the period of March 4–10, 2022, a total of 1,888 cases and 55 deaths were recorded across health districts in all 10 regions, for an estimated national population of 17,395,035 in 2021[1]. The report indicates that 24 health districts were affected, 18 of which remained active, with the most impacted regions being the Centre, Littoral, South, South-West, and North. The median age of patients was 25 years (range: 0–89 years), with a sex ratio of two females to one male. More recently, Report No. 43 on cholera management for the period of May 16–30, 2023, documented 1,070 cases in three active regions (Centre, Littoral, and South), including 26 deaths. The median age of patients was 28 years (range: 0–103 years), with a sex ratio of one female to three males. Figure 1 illustrates the Cameroonian health districts affected by cholera and highlights those most severely impacted during these outbreaks.

[1] www.ccousp.cm/documentations/rapports-de-situation-cholera.

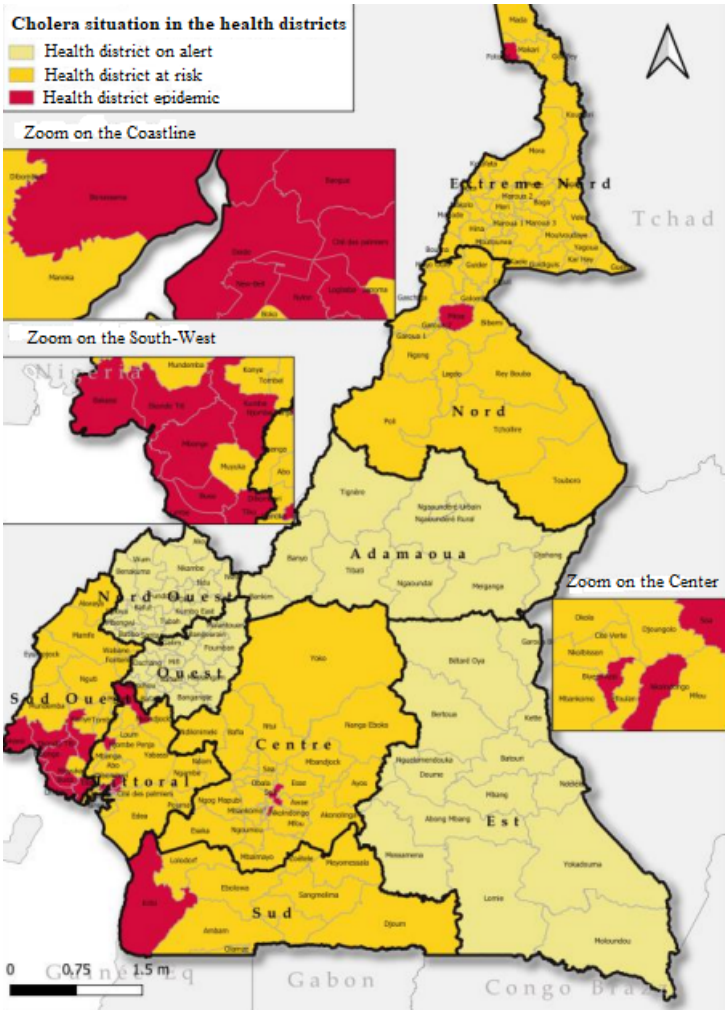

Figure 1: The different Health Districts affected in the affected regions in Cameroon from 10 March 2022 (see https://www.ccousp.cm/documentations/rapports-de-situation-can/).

According to Radio France Internationale (RFI) [9], authorities said on April 19, 2023, that the Center region, whose capital is the country's capital Yaoundé, "has been experiencing a resurgence of cholera cases for the past four weeks" and confirmed 88 cases and five (5) deaths to date, without specifying which localities were most affected. The Ministry of Health stated that the response system for this outbreak had been initiated, and that the disease had "resurgence" in this region over the last four weeks.

Fractional calculus, a topic originating from L'Hôpital's question about the meaning of a half-order derivative, has been widely explored by researchers in fields such as biology, physics, ecology, and engineering to better capture real-world processes [10–13]. Cholera has also been extensively studied, with mathematical models used to understand its transmission dynamics and to design effective control strategies [14–16]. Most cholera models are based on integer-order ordinary differential equations, which neglect memory and the nonlocal characteristics of epidemic systems. Fractional-order differential systems have been proposed to better represent epidemic behavior [11, 17, 18]. As a result, a wide range of mathematical cholera models has been developed, involving both ordinary and fractional differential equations (ODEs and FDEs) [14–16, 19–25].

In [19], Lemos-Paiao et al. proposed a mathematical model for cholera that included the effects of vaccination. In [14], Capasso and Paveri-Fontana developed a model for the 1973 cholera pandemic in the European Mediterranean region. In [20], Codeço applied a classical SIR epidemiological model to account for the impact of *Vibrio cholerae* on aquatic resources. Building on this, Hartley et al. [21] extended and analyzed the model in [20] by incorporating the pathogen's hyperinfectivity. Mukandavire et al. [22] proposed a cholera model with dual transmission routes, using bilinear incidence rates for both direct and environmental infections, but without accounting for saturation effects. Chen et al. [23] developed a partial differential equation model to assess the roles of human diffusion and bacterial convection in cholera transmission, and examined the multiple factors influencing the spatial distribution of the disease. Hoskova-Mayerova [24] designed an optimal control model for cholera epidemics, showing that four investigated control strategies could significantly limit or eliminate cholera in asymptomatic populations. Monje et al. [25] investigated a prolonged cholera outbreak caused by contaminated stream water in the Kyangwali refugee camp, Hoima District, Western Uganda. Muhammad [16] studied bifurcation analysis for a co-infection model of Buruli ulcer and cholera, identifying the possibility of backward bifurcation. Subchan [26] introduced a SEIQR model to optimize cholera transmission dynamics by explicitly including bacterial concentration. Finally, Ozkose et al. [15] employed a fractional-order model to analyze COVID-19 and cholera outbreaks in Congo, making an important contribution to cholera epidemic modeling.

In this study, we propose a $\mathcal{SITRV}-\mathcal{B}$ (Susceptible–Infectious–Treated–Recovered–Vaccinated–Bacterial) model that incorporates both human-to-human and environmental transmission using standard incidence rates and fractional derivatives. We begin by presenting key definitions of fractional derivatives in the Caputo sense, along with a fundamental theoretical result. We then formulate the model and demonstrate that its solutions are bounded. Using the next-generation method, we compute the basic reproduction number $\mathcal{R}_c$ and establish the stability of the cholera-free equilibrium by showing that the Jacobian matrix evaluated at this equilibrium has all eigenvalues with negative real parts. We also prove the existence and uniqueness of solutions, followed by model calibration, sensitivity analysis, and forecasting. For simulation, we implement a numerical scheme based on the Adams–Bashforth–Moulton method and explore two scenarios: one with fixed transmission parameters and another with time-varying parameters. In both cases, we conclude that the disease persists when the control reproduction number exceeds one, and the model admits periodic solutions.

The remainder of this work is organized as follows. Section 2 introduces the Caputo fractional-order derivative and presents the model formulation. Section 3 investigates the non-negativity and boundedness of solutions, the existence and uniqueness of solutions, the asymptotic stability of the cholera-free equilibrium, and the existence of at least one endemic equilibrium point. This section also covers model calibration, forecasting, sensitivity analysis, and the construction of a numerical scheme for simulation. Section 4 is devoted to discussion, and the paper concludes with final remarks.

2 Material and methods

2.1 Preliminary definitions of Caputo fractional order derivative

A fractional order refers to an order of a derivative or integral that is not a whole number but a fractional or decimal number. This concept is used in various fields such as system dynamics, control theory, fractional calculus, and banking systems. In this part, we give some definitions of the Caputo-order derivative.

Definition 1 (The Riemann-Liouville integral R-L [10]). *Let $h \in C([a,b])$; the fractional Riemann-Liouville integral of the function h of order $\iota > 0$ is defined by:*

$$\mathcal{J}_a^{\iota} h(x) = \frac{1}{\Gamma(\iota)} \int_a^x (-s+x)^{-1+\alpha} h(s) ds. \qquad \iota \notin \mathbb{N} \tag{1}$$

Definition 2 (Caputo derivative [10]). *Let $h \in \mathcal{C}^l([0;d])$, $d > 0$, $\iota \in \mathbb{R}$, $l \in \mathbb{N}$ be such that $l-1 < \iota < l$. The Caputo fractional-order derivative of order ι of h is given by:*

$$ {}_0^C\mathcal{D}_t^{\iota}\left(h(s)\right) = \frac{1}{\Gamma(l-\iota)} \int_0^s (s-\varpi)^{l-\iota-1} h^{(l)}(\varpi)\, d\varpi, \quad s > 0. \tag{2}$$

If fractional order $\iota = 1$, then ${}_0^C\mathcal{D}_t^{\iota}(\bullet) = \dfrac{d}{dt}(\bullet)$.

2.2 Model formulation

Here, we build our model by extending the one proposed by Ana P. Lemos-Paiao et *al.* [19]. The model is a Susceptible-Infected-Treated-Recovered-Vaccinated-Bacteria ($\mathcal{SITRV}-\mathcal{B}$) compartmental model and considers a class of bacterial concentration and direct transmission between human hosts. We denote by $\mathcal{N}(t)$ the total human population at any time t by $\mathcal{N}(t) = \mathcal{S}(t) + \mathcal{I}(t) + \mathcal{T}(t) + \mathcal{R}(t) + \mathcal{V}(t)$, where $\mathcal{S}(t)$, $\mathcal{I}(t)$, $\mathcal{T}(t)$, $\mathcal{R}(t)$, and $\mathcal{V}(t)$, denote respectively, susceptible humans, infectious humans, infected humans who received treatment, recovered humans, and vaccinated humans. Susceptible humans increase through a constant recruitment rate Λ and decrease due to infection, which can be contracted through contaminated food or water, and through direct contact with infected individuals $\mathcal{I}$, at a rate $\alpha\dfrac{\mathcal{B}(t)}{k+\mathcal{B}(t)}$ and $\psi\dfrac{\mathcal{I}(t)}{\mathcal{N}(t)}$, respectively. $1/\mu$ represents the life span of humans. After contact with an infectious individual and / or an infected material, susceptible humans become infected and therefore receive treatment at a rate c. Without successful treatment, an infected individual can die from infection at an additional rate d_1. The treated individuals recover at a rate e and lose immunity at a rate a_1 and become susceptible again. A rate b of susceptible humans receive a vaccine. In this work, we suppose that vaccine is perfect.

Table 1: Definitions of symbols used in equation (3).

Symbols	**Definitions**
Λ	Recruitment rate of sensitive populations
α	Indirect infection rate
μ	The natural mortality rate
k	The half saturation constant
a_1	Recovered populations can lose their immunity
a_2	Vaccinated populations can lose their immunity
b	Vaccine coverage
c	The infected populations can get a proper treatment,
e	The rate of people undergoing re-establishment treatment
d_1,d_2	Disease-related death rates
γ	The rate of infected populations who lead to a rise in the bacterial concentration.
ψ	Direct transmission rate
θ	Bacterial decay rate

Using the Caputo derivative operator, our model described above is as follows:

$$\begin{cases} \mathcal{H}^{\chi-1} \times_0^C \mathcal{D}_t^{\chi} \mathcal{S}(t) &= \Lambda - \left(\dfrac{\alpha \mathcal{B}(t)}{\mathcal{B}(t)+k} + \psi \dfrac{\mathcal{I}(t)}{\mathcal{N}(t)}\right) \mathcal{S}(t) + a_1 \mathcal{R}(t) + a_2 \mathcal{V}(t) - \overbrace{(b+\mu)}^{k_1} \mathcal{S}(t), \\ \mathcal{H}^{\chi-1} \times_0^C \mathcal{D}_t^{\chi} \mathcal{I}(t) &= \left(\dfrac{\alpha \mathcal{B}(t)}{\mathcal{B}(t)+k} + \psi \dfrac{\mathcal{I}(t)}{\mathcal{N}(t)}\right) \mathcal{S}(t) - \overbrace{(c+d_1+\mu)}^{k_2} \mathcal{I}(t), \\ \mathcal{H}^{\chi-1} \times_0^C \mathcal{D}_t^{\chi} \mathcal{T}(t) &= c\mathcal{I}(t) - \overbrace{(e+d_2+\mu)}^{k_3} \mathcal{T}(t), \\ \mathcal{H}^{\chi-1} \times_0^C \mathcal{D}_t^{\chi} \mathcal{R}(t) &= e\mathcal{T}(t) - \overbrace{(a_1+\mu)}^{k_4} \mathcal{R}(t), \\ \mathcal{H}^{\chi-1} \times_0^C \mathcal{D}_t^{\chi} \mathcal{V}(t) &= b\mathcal{S}(t) - \overbrace{(a_2+\mu)}^{k_5} \mathcal{V}(t), \\ \mathcal{H}^{\chi-1} \times_0^C \mathcal{D}_t^{\chi} \mathcal{B}(t) &= \gamma \mathcal{I}(t) - \theta \mathcal{B}(t), \end{cases} \tag{3}$$

where ${}_0^C\mathcal{D}_t^{\chi}$ denotes the fractional order derivative in the Caputo sense of order χ. The following initial conditions are associated with the system (3): $\mathcal{S}(0) = \mathcal{S}_0 > 0$, $\mathcal{I}(0) = \mathcal{I}_0 \geq 0$, $\mathcal{T}(0) = \mathcal{T}_0 \geq 0$, $\mathcal{R}(0) = \mathcal{R}_0 \geq 0$, $\mathcal{V}(0) = \mathcal{V}_0 \geq 0$, $\mathcal{B}(0) = \mathcal{B}_0 \geq 0$.

All symbols used in the model are defined in the table 1. Figure 2 displays the Cholera transmission dynamics.

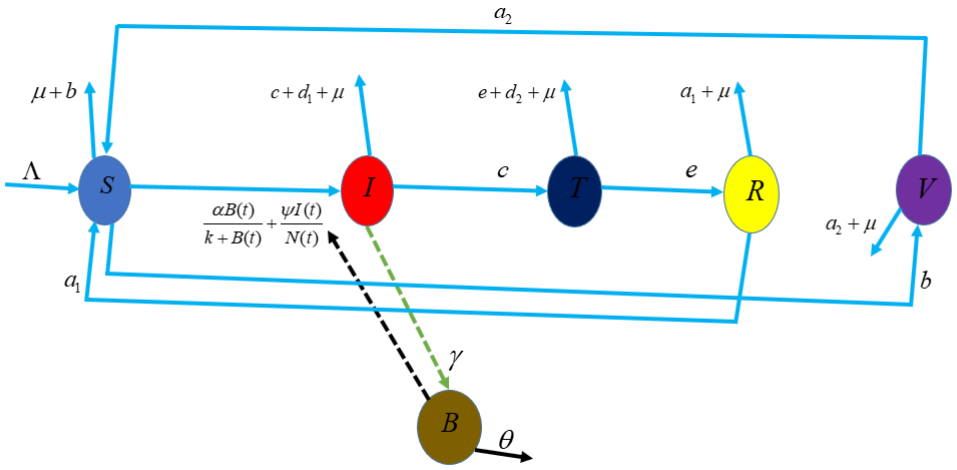

Figure 2: Compartmental diagram of the Cholera transmission dynamics.

3 Results

3.1 Nonnegativity and boundedness of solutions

In what follows, we will determine the boundedness of model variables under nonnegative circumstances. To establish the domain, the variables $\mathcal{S}(t), \mathcal{I}(t), \mathcal{T}(t), \mathcal{R}(t), \mathcal{V}(t), \mathcal{B}(t)$ must be positive for all $t \geq 0$.

Let's assume that the total human population at any time t is given by:

$$\mathcal{N}(t) = \mathcal{S}(t) + \mathcal{I}(t) + \mathcal{T}(t) + \mathcal{R}(t) + \mathcal{V}(t).$$

Adding the first five equation of model (3), with $\chi = 1$, we obtain:

$$\begin{aligned} {}_0^C\mathcal{D}_t^{\chi}\mathcal{N} &= {}_0^C\mathcal{D}_t^{\chi}\left(\mathcal{S}+\mathcal{I}+\mathcal{T}+\mathcal{R}+\mathcal{V}\right), \\ &= \Lambda - \mu\left[\mathcal{S}+\mathcal{I}+\mathcal{T}+\mathcal{R}+\mathcal{V}\right] - d_1\mathcal{I} - d_2\mathcal{T}, \\ &= \Lambda - \mu\mathcal{N} - d_1\mathcal{I} - d_2\mathcal{T}, \\ &\leq -\mu\mathcal{N} + \Lambda. \end{aligned}$$

Solving this equation gives

$$\mathcal{N}(t) \leq \frac{\Lambda}{\mu} + \left(\mathcal{N}(0) - \frac{\Lambda}{\mu}\right) e^{-\mu t}, \quad \forall t \geq 0.$$

with $N(0) = \mathcal{S}(0) + \mathcal{I}(0) + \mathcal{T}(0) + \mathcal{R}(0) + \mathcal{V}(0)$. Thus, $\limsup_{t\to+\infty} \mathcal{N}(t) \leq \frac{\Lambda}{\mu}$, which means that $\mathcal{N}(t) = \mathcal{S}(t) + \mathcal{I}(t) + \mathcal{T}(t) + \mathcal{R}(t) + \mathcal{V}(t) \leq \frac{\Lambda}{\mu}$, $\forall t \geq 0$.

In the same idea, with $\mathcal{I}(t) \leq \Lambda\mu^{-1}$, it follows that

$$ {}_0^C\mathcal{D}_t^{\chi}\mathcal{B}(t) = \gamma\mathcal{I}(t) - \theta\mathcal{B}(t) \leq \gamma\Lambda\mu^{-1} - \theta\,\mathcal{B}(t), $$

which gives

$$ \mathcal{B}(t) \leq \frac{\gamma\,\Lambda}{\mu\,\theta} + \left(\mathcal{B}(0) - \frac{\gamma\,\Lambda}{\mu\theta}\right) e^{-\theta t}, \quad \forall t \geq 0. $$

Thus $\limsup_{t\to+\infty} \mathcal{B}(t) \leq \frac{\gamma\,\Lambda}{\mu\,\theta}$, that is $\mathcal{B}(t) \leq \frac{\gamma\,\Lambda}{\mu\,\theta}$, $\forall t \geq 0$. This demonstrates that the model (3) has bounded solutions, which are specified in the compact and absorbing set:

$$ \Sigma = \left\{(\mathcal{S},\mathcal{I},\mathcal{T},\mathcal{R},\mathcal{V},\mathcal{B})' \in \mathbb{R}_+^6 : \quad \mathcal{N} \leq \frac{\Lambda}{\mu}; \mathcal{B} \leq \frac{\gamma\Lambda}{\mu\,\theta}\right\}. \tag{4} $$

Note that for $0 < \chi < 1$, $e^{-\mu t}$ (resp. $e^{-\theta t}$) is replaced by the Mittag-Leffler function $E_{\chi}(m) = \sum_{k=0}^{+\infty} \frac{m^{\chi}}{\Gamma(1+k\chi)}$ [27], with $E_1(m) = e^m$.

3.2 Existence and uniqueness of Solution

The validity and reliability of the model (3) give the essential mathematical assurance, defining the findings of existence and uniqueness in epidemic modeling. Now, suppose $\chi = 1$. Let's define a reasonable set of state variables as

$$ \varpi = \left\{(\mathcal{S},\mathcal{I},\mathcal{T},\mathcal{R},\mathcal{V},\mathcal{B}) \in \mathbb{R}_+^6 : \max\left\{|\mathcal{S}|,|\mathcal{I}|,|\mathcal{T}|,|\mathcal{R}|,|\mathcal{V}|,|\mathcal{B}|\right\} \leq \mathcal{P}\right\}. $$

where, $\mathcal{P} \in \mathbb{R}$. Let us consider the differential equation,

$$ D_t^{\chi}G(t) = J(t,G(t)), \quad 0 \leq t_0 \leq T < \infty, \tag{5} $$

with initial condition $G(t_0) = G_0$, where $\chi \in (0,1]$ and $J : ([0,T] \times \varpi \longrightarrow \mathbb{R})$. The solution of the equation (5) is

$$ G(t) = G_0(t) + \frac{1}{\Gamma(\chi)} \int_0^t (t-\eta)^{\chi-1} J(\eta, G(\eta))d\eta. $$

where

$$G(t)=\begin{pmatrix}\mathcal{S}(t)\\ \mathcal{I}(t)\\ \mathcal{T}(t)\\ \mathcal{R}(t)\\ \mathcal{V}(t)\\ \mathcal{B}(t)\end{pmatrix},\ G_0(t)=\begin{pmatrix}\mathcal{S}_0(t)\\ \mathcal{I}_0(t)\\ \mathcal{T}_0(t)\\ \mathcal{R}_c(t)\\ \mathcal{V}_0(t)\\ \mathcal{B}_0(t)\end{pmatrix}\ \text{and}\ J(t,G(t))=\mathcal{H}^{\chi-1}\times\begin{pmatrix}J_1\\ J_2\\ J_3\\ J_4\\ J_5\\ J_6\end{pmatrix}.$$

with $J_1=\Lambda-\left(\frac{\alpha\mathcal{B}}{k+\mathcal{B}}+\psi\frac{\mathcal{I}}{N}\right)\mathcal{S}+a_1\mathcal{R}+a_2\mathcal{V}-k_1\mathcal{S}$, $J_2=\left(\frac{\alpha\mathcal{B}}{k+\mathcal{B}}+\psi\frac{\mathcal{I}}{N}\right)\mathcal{S}-k_2\mathcal{I}$, $J_3=c\mathcal{I}-k_3\mathcal{T}$, $J_4=e\mathcal{T}-k_4\mathcal{R}$, $J_5=b\mathcal{S}-k_5\mathcal{V}$ and $J_6=\gamma\mathcal{I}-\theta\mathcal{B}$.

with $k_1=b+\mu$, $k_2=c+d_1+\mu$, $k_3=e+d_2+\mu$, $k_4=a_1+\mu$ and $k_5=a_2+\mu$.

Let $\mathcal{C}=J([0,T]\times\varpi,\mathbb{R})$ a Banach space endowed with the following norm:

$$\|G\|=\|(\mathcal{S},\mathcal{I},\mathcal{T},\mathcal{R},\mathcal{V},\mathcal{B})\|=\sup_{t\in[0,t_f]}|G(t)|,$$

where, $|G(t)|=\{|\mathcal{S}|+|\mathcal{I}|+|\mathcal{T}|+|\mathcal{R}|+|\mathcal{V}|+|\mathcal{B}|\}$, $(\mathcal{S},\mathcal{I},\mathcal{T},\mathcal{R},\mathcal{V},\mathcal{B})\in J([0,T]\times\varpi,\mathbb{R})$. We have the following result:

Lemma 1. *In the Banach space $\mathcal{C}$, all kernels J_j meet the Lipschitz condition, where $j=1,2,...,6$.*

Proof. Let $G(t), \overline{G(t)} \in J$.

$$
\begin{aligned}
&\left|J_1(t,G(t)) - J_1(t,\overline{G(t)})\right| \\
&= \left|\Lambda - \left(\alpha\frac{\mathcal{B}(t)}{k+\mathcal{B}(t)} + \psi\frac{\mathcal{I}(t)}{\mathcal{N}(t)} + k_1\right)\mathcal{S}(t) + a_1\mathcal{R}(t) + a_2\mathcal{V}(t)\right. \\
&\quad \left. -\Lambda + \left(\alpha\frac{\overline{\mathcal{B}}(t)}{k+\overline{\mathcal{B}}(t)} + \psi\frac{\overline{\mathcal{I}}(t)}{\overline{N}(t)} + k_1\right)\overline{\mathcal{S}(t)} - a_1\overline{\mathcal{R}}(t) - a_2\overline{\mathcal{V}}(t)\right|, \\
&\leq \frac{\alpha\left|B(K+\overline{\mathcal{B}})\right|}{\left|(k+\mathcal{B}(t))(k+\overline{\mathcal{B}}(t))\right|}\left|\mathcal{S}(t)-\overline{\mathcal{S}}(t)\right| + \frac{\alpha k\left|\overline{\mathcal{B}}(t)\right|}{\left|(k+\mathcal{B}(t))(k+\overline{\mathcal{B}}(t))\right|}\left|\mathcal{B}(t)-\overline{\mathcal{B}}(t)\right| \\
&\quad + \frac{\psi\left|\mathcal{I}\mathcal{S}-N\mathcal{I}\right|}{\left|N\overline{N}\right|}\left|\mathcal{S}(t)-\overline{\mathcal{S}(t)}\right| + \frac{\psi\left|\mathcal{I}\mathcal{S}-N\overline{\mathcal{S}}\right|}{\left|N\overline{N}\right|}\left|\mathcal{I}(t)-\overline{\mathcal{I}}(t)\right| \\
&\quad + \frac{\psi\left|\mathcal{I}\mathcal{S}\right|}{\left|N\overline{N}\right|}\left|\mathcal{T}(t)-\overline{\mathcal{T}(t)}\right| + \frac{\psi\left|\mathcal{I}\mathcal{S}\right|}{\left|N\overline{N}\right|}\left|\mathcal{R}(t)-\overline{\mathcal{R}(t)}\right| + \frac{\psi\left|\mathcal{I}\mathcal{S}\right|}{\left|N\overline{N}\right|}\left|\mathcal{V}(t)-\overline{\mathcal{V}(t)}\right| \\
&\quad + k_1\left|\mathcal{S}(t)-\overline{\mathcal{S}(t)}\right| + a_1\left|\mathcal{R}(t)-\overline{\mathcal{R}}(t)\right| + a_2\left|\mathcal{V}(t)-\overline{\mathcal{V}}(t)\right| \\
&\leq \left(\frac{\alpha\left|B(K+\overline{\mathcal{B}})\right|}{\left|(k+\mathcal{B}(t))(k+\overline{\mathcal{B}}(t))\right|} + \frac{\psi\left|\mathcal{I}\mathcal{S}-N\mathcal{I}\right|}{\left|N\overline{N}\right|} + k_1\right)\left|\mathcal{S}(t)-\overline{\mathcal{S}(t)}\right| \\
&\quad + \frac{\psi\left|\mathcal{I}\mathcal{S}-N\overline{\mathcal{S}}\right|}{\left|N\overline{N}\right|}\left|\mathcal{I}(t)-\overline{\mathcal{I}}(t)\right| + \frac{\psi\left|\mathcal{I}\mathcal{S}\right|}{\left|N\overline{N}\right|}\left|\mathcal{T}(t)-\overline{\mathcal{T}(t)}\right| \\
&\quad + \left(\frac{\psi\left|\mathcal{I}\mathcal{S}\right|}{\left|N\overline{N}\right|} + a_1\right)\left|\mathcal{R}(t)-\overline{\mathcal{R}}(t)\right| + \left(\frac{\psi\left|\mathcal{I}\mathcal{S}\right|}{\left|N\overline{N}\right|} + a_2\right)\left|\mathcal{V}(t)-\overline{\mathcal{V}}(t)\right| \\
&\quad + \frac{\alpha k\left|\overline{\mathcal{B}}(t)\right|}{\left|(k+\mathcal{B}(t))(k+\overline{\mathcal{B}}(t))\right|}\left|\mathcal{B}(t)-\overline{\mathcal{B}}(t)\right| \\
&\leq l_1\left(\left|\mathcal{S}(t)-\overline{\mathcal{S}(t)}\right| + \left|\mathcal{I}(t)-\overline{\mathcal{I}(t)}\right\| + \left|\mathcal{T}(t)-\overline{\mathcal{T}(t)}\right| + \left|\mathcal{R}(t)-\overline{\mathcal{R}(t)}\right|\right. \\
&\qquad \left. + \left|\mathcal{V}(t)-\overline{\mathcal{V}(t)}\right| + \left|\mathcal{B}(t)-\overline{\mathcal{B}(t)}\right|\right),
\end{aligned}
$$

where

$$
\begin{aligned}
l_1 &= k_1 + a_1^{\chi} + a_2^{\chi} + \\
&\quad + \max_{t\in[0;t_f]}\left\{\frac{\alpha^{\chi}\left|B(K+\overline{\mathcal{B}})\right|}{\left|(k+\mathcal{B}(t))(k+\overline{\mathcal{B}}(t))\right|} + \frac{\psi^{\chi}\left|\mathcal{I}\mathcal{S}-N\mathcal{I}\right|}{\left|N\overline{N}\right|}, \frac{\psi^{\chi}\left|\mathcal{I}\mathcal{S}-N\overline{\mathcal{S}}\right|}{\left|N\overline{N}\right|}, \frac{\psi^{\chi}\left|\mathcal{I}\mathcal{S}\right|}{\left|N\overline{N}\right|},\right. \\
&\qquad \left.\frac{\psi^{\chi}\left|\mathcal{I}\mathcal{S}\right|}{\left|N\overline{N}\right|}, \frac{\psi^{\chi}\left|\mathcal{I}\mathcal{S}\right|}{\left|N\overline{N}\right|}, \frac{\alpha^{\chi}k\left|\overline{\mathcal{B}}(t)\right|}{\left|(k+\mathcal{B}(t))(k+\overline{\mathcal{B}}(t))\right|}\right\}.
\end{aligned}
$$

$$
\begin{aligned}
&\left|J_2(t,G(t))-J_2(t,\overline{G(t)})\right| \\
&=\left|\alpha^{\chi}\frac{\mathcal{B}(t)}{k+\mathcal{B}(t)}\mathcal{S}(t)+\psi^{\chi}\frac{\mathcal{S}(t)}{\mathcal{N}(t)}\mathcal{I}(t)-k_2\mathcal{I}(t)-\alpha^{\chi}\frac{\overline{\mathcal{B}(t)}}{k+\overline{\mathcal{B}(t)}}\overline{\mathcal{S}}(t)-\psi^{\chi}\frac{\overline{\mathcal{S}}(t)}{\overline{\mathcal{N}}(t)}\overline{\mathcal{I}(t)}+k_2\overline{\mathcal{I}(t)}\right| \\
&\leq\left(\frac{\alpha^{\chi}\left|\mathcal{B}(k+\overline{\mathcal{B}})\right|}{\left|(k+\mathcal{B})(k+\overline{\mathcal{B}})\right|}+\psi^{\chi}\left|\frac{\overline{\mathcal{I}}}{\overline{\mathcal{N}}}-\frac{\mathcal{S}\mathcal{I}}{\mathcal{N}\overline{\mathcal{N}}}\right|\right)\left\|\mathcal{S}(t)-\overline{\mathcal{S}(t)}\right| \\
&\quad+\left(k_2+\psi^{\chi}\left|\frac{\overline{\mathcal{S}}}{\overline{\mathcal{N}}}-\frac{\mathcal{S}\mathcal{I}}{\mathcal{N}\overline{\mathcal{N}}}\right|\right)\left|\mathcal{I}(t)-\overline{\mathcal{I}(t)}\right| \\
&\quad+\psi^{\chi}\left|\frac{\mathcal{S}\mathcal{I}}{\mathcal{N}\overline{\mathcal{N}}}\right|\left|\mathcal{T}(t)-\overline{\mathcal{T}(t)}\right|+\psi^{\chi}\left|\frac{\mathcal{S}\mathcal{I}}{\mathcal{N}\overline{\mathcal{N}}}\right|\left|\mathcal{R}(t)-\overline{\mathcal{R}(t)}\right|+\psi^{\chi}\left|\frac{\mathcal{S}\mathcal{I}}{\mathcal{N}\overline{\mathcal{N}}}\right|\left|\mathcal{V}(t)-\overline{\mathcal{V}(t)}\right| \\
&\quad+\frac{\alpha^{\chi}k\left|\overline{\mathcal{S}}\right|}{\left|(k+\mathcal{B})(k+\overline{\mathcal{B}})\right|}\left|\mathcal{B}-\overline{\mathcal{B}}\right| \\
&\leq l_2\left(\left|\mathcal{S}(t)-\overline{\mathcal{S}(t)}\right|+\left|\mathcal{I}(t)-\overline{\mathcal{I}(t)}\right|+\left|\mathcal{T}(t)-\overline{\mathcal{T}(t)}\right|+\left|\mathcal{R}(t)-\overline{\mathcal{R}(t)}\right|+\left|\mathcal{V}(t)-\overline{\mathcal{V}(t)}\right|\right. \\
&\qquad\left.+\left|\mathcal{B}(t)-\overline{\mathcal{B}(t)}\right|\right),
\end{aligned}
$$

where

$$
l_2=k_2+\max_{t\in[0,t_f]}\left\{\frac{\alpha^{\chi}\left|\mathcal{B}\right|}{\left|(k+\mathcal{B})\right|}+\psi^{\chi}\left|1-\frac{\mathcal{S}\mathcal{I}}{\mathcal{N}\overline{\mathcal{N}}}\right|,\psi^{\chi}\left|1-\frac{\mathcal{S}\mathcal{I}}{\mathcal{N}\overline{\mathcal{N}}}\right|,\psi^{\chi}\left|\frac{\mathcal{S}\mathcal{I}}{\mathcal{N}\overline{\mathcal{N}}}\right|,\frac{\alpha^{\chi}k\left|\overline{\mathcal{S}}\right|}{\left|(k+\mathcal{B})(k+\overline{\mathcal{B}})\right|}\right\}
$$

With the same reasoning, we obtain for the remaining kernels:

$$
\begin{aligned}
\left|J_3(t,G(t))-J_3(t,\overline{G(t)})\right|&\leq c^{\chi}\left|\mathcal{I}(t)-\overline{\mathcal{I}(t)}\right|+l_3\left|\mathcal{T}(t)-\overline{\mathcal{T}(t)}\right|, \\
\left|J_4(t,G(t))-J_4(t,\overline{G(t)})\right|&\leq l_4\left|\mathcal{R}(t)-\overline{\mathcal{R}(t)}\right|, \\
\left|J_5(t,G(t))-J_5(t,\overline{G(t)})\right|&\leq l_5\left|\mathcal{V}(t)-\overline{\mathcal{V}(t)}\right|, \\
\left|J_6(t,G(t))-J_6(t,\overline{G(t)})\right|&\leq l_6\left|\mathcal{B}(t)-\overline{\mathcal{B}(t)}\right|,
\end{aligned}
$$

with $l_3=c^{\chi}+k_3^{\chi}$, $l_4=e^{\chi}+k_4^{\chi}$, $l_5=b^{\chi}+k_5^{\chi}$, and $l_6=\gamma^{\chi}+\theta^{\chi}$.

It then follows that

$$
\left\|J(t,G(t))-J(t,\overline{G(t)})\right\|=\sup_{t\in[0,t_f]}\sum_{i=1}^{6}\left|J_i(t,G(t))-J_i(t,\overline{G(t)})\right|\leq\delta\left\|G(t)-\overline{G(t)}\right\|
$$

which, $\delta=max\left\{l_j,j=1,2,...,6\right\}$. Hence, $J(t,G(t))$ satisfies the Lipschitz condition on $\mathcal{C}$. This shows that the model (3) has at least one solution. □

Lemma 2. *The solutions of equations* (3) *are unique if* $\dfrac{\delta t_f^{\chi}}{\chi\Gamma(\chi)}<1$.

Proof. Let us defined the linear mapping $\mathcal{N}:\mathcal{C}\longrightarrow\mathcal{C}$ as follow:

$$
\mathcal{N}(G(t))=G_0(t)+\frac{1}{\Gamma(\chi)}\int_{\cdot 0}^{t}(-\eta+t)^{-1+\chi}J(\eta,G(\eta))d\eta. \tag{6}
$$

where $G(t) = \mathcal{N}(G(t))$ is the solution of (5). For $G(t), \overline{G(t)} \in \mathcal{C}$, it follows that

$$\begin{aligned}
\left\|\mathcal{N}(G(t)) - \mathcal{N}(\overline{G(t)})\right\| &= \left\|\frac{1}{\Gamma(\chi)}\int_0^t (t-\eta)^{\chi-1}\left(J(\eta, G(\eta)) - J(\eta, \overline{G(\eta)})\right)d\eta\right\|, \\
&\leq \frac{1}{\Gamma(\chi)}\int_0^t (t-\eta)^{\chi-1}\left\|J(\eta, G(\eta)) - J(\eta, \overline{G(\eta)})\right\|d\eta, \\
&\leq \frac{\delta}{\Gamma(\chi)}\int_0^t (t-\eta)^{\chi-1}\left\|G(\eta) - \overline{G(\eta)}\right\|d\eta, \quad \text{From Lemma 1,} \\
&= \frac{\delta t_f^{\chi}}{\chi\Gamma(\chi)}\left\|G(\eta) - \overline{G(\eta)}\right\|.
\end{aligned}$$

Thus, $\mathcal{N}$ is a contraction, if $1 > \dfrac{\delta t_f^{\chi}}{\chi\Gamma(\chi)}$. The uniqueness of solution come from the Banach contraction theorem [28]. □

3.3 Asymptotic stability

3.3.1 The Cholera-free equilibrium and the basic reproduction number

The fundamental reproduction number, $\mathcal{R}_c$, is a mathematical term used in epidemiology to measure the spread of a disease within a population. It is crucial for assessing the infectiousness and speed of disease spread. If $\mathcal{R}_c$ is higher, the disease spreads more, while if it's lower, it dies out. Factors influencing this number include disease transmission mode, pathogen infectiousness, and social and environmental factors.

Pauline van den Driessche in [29] describes the Next-Generation Matrix Method (NGMM) as follows:

The NGMM $\mathcal{G}$ is defined as FV^{-1}, where FV^{-1} represents the rate of new infections in compartment i, and V_i represents the rate of transfer of individuals into and out of the it compartment.

$$F = \left[\frac{\partial F_i(x_0)}{\partial x_j}\right] \quad and \quad V = \left[\frac{\partial V_i(x_0)}{\partial x_j}\right] \quad for \quad 1 \leq i, \quad j \leq m.$$

where x_0 is the disease-free equilibrium state.

Then, the control reproduction number denoted to $\mathcal{R}_c$ is the Cholera-free equilibrium (CFE) state is the dominant eigenvalue of matrix $\mathcal{G} = FV^{-1}$. Such that:

$$\mathcal{R}_c = \rho\left(FV^{-1}\right).$$

where ρ denotes the spectral radius.

Since just the infection states are required and all other states that are not disease compartments are disregarded, the next-generation matrix is far easier to employ than Jacobian-based methods.

By following the instructions in this method, we obtain the mathematical expression for our model at the Cholera-free equilibrium denoted by $\xi^0 = \left(\mathcal{S}^0; \mathcal{I}^0; \mathcal{T}^0; \mathcal{R}^0; \mathcal{V}^0; \mathcal{B}^0\right) = \left(\dfrac{\Lambda\, k_5}{k_1\, k_5 - b\, a_2}, 0, 0, 0, \dfrac{\Lambda\, b}{k_1\, k_5 - b\, a_2}, 0\right)$.

The Jacobian matrix of our model (3) is represented by:

$$J = \begin{pmatrix} -\left[\frac{\alpha\mathcal{B}}{k+\mathcal{B}} + \frac{\psi\mathcal{I}(N-\mathcal{S})}{N^2} + k_1\right] & -\left(\frac{\psi\mathcal{S}(N-\mathcal{I})}{N^2}\right) & \left[\frac{\psi\mathcal{I}\mathcal{S}}{N^2} + a_1\right] & \left[\frac{\psi\mathcal{I}\mathcal{S}}{N^2} + a_2\right] & -\left[\frac{\alpha\mathcal{S}k}{(k+\mathcal{B})^2}\right] & -\frac{k\mathcal{S}}{(k+\mathcal{B})^2} \\ \left[\frac{\alpha\,\mathcal{B}}{k+\mathcal{B}} + \frac{\psi\mathcal{I}(N-\mathcal{S})}{N^2}\right] & \left[\frac{\psi\mathcal{S}(N-\mathcal{I})}{N^2} - k_2\right] & 0 & 0 & 0 & \frac{\alpha\mathcal{S}k}{(k+\mathcal{B})^2} \\ 0 & c & -k_3 & 0 & 0 & 0 \\ 0 & 0 & e & -k_4 & 0 & 0 \\ b & 0 & 0 & 0 & -k_5 & 0 \\ 0 & \gamma & 0 & 0 & 0 & -\theta \end{pmatrix}$$

Taking into account the compartments of the infected at the Cholera-free equilibrium, this Jacobian matrix gives us:

$$J_{CFE} = \begin{pmatrix} \frac{\psi\,\mathcal{S}^0}{N^0} - k_2 & 0 & \frac{\alpha\,\mathcal{S}^0}{k} \\ c & -k_3 & 0 \\ \gamma & 0 & -\theta \end{pmatrix}$$

Then, from model system (3), we have:

$$\frac{dx}{dt} = F(x) - V(x) \quad with \quad x \;= (\mathcal{S}(t); \mathcal{I}(t); \mathcal{T}(t); \mathcal{R}(t); \mathcal{V}(t); \mathcal{B}(t))^T.$$

Where the Jacobian matrices at the CFE of $F(x)$ and of $V(x)$ are, respectively, given by:

$$F = \begin{pmatrix} \frac{\psi\,\mathcal{S}^0}{N^0} & 0 & \frac{\alpha\,\mathcal{S}^0}{k} \\ 0 & 0 & 0 \\ 0 & 0 & 0 \end{pmatrix} \quad and \quad V = \begin{pmatrix} k_2 & 0 & 0 \\ -c & k_3 & 0 \\ -\gamma & 0 & \theta \end{pmatrix}$$

$$FV^{-1} = \begin{pmatrix} \frac{S^0\,\alpha\,\gamma}{k_2\,k\,\theta} + \frac{S^0\,\psi}{N^0\,k_2} & 0 & \frac{S^0\,\alpha}{k\,\theta} \\ 0 & 0 & 0 \\ 0 & 0 & 0 \end{pmatrix}$$

$$det\left(FV^{-1} - \mathcal{R}_c I\right) = \begin{pmatrix} \frac{S^0\,\alpha\,\gamma}{k_2\,k\,\theta} + \frac{S^0\,\psi}{N^0\,k_2} - \mathcal{R}_c & 0 & \frac{S^0\,\alpha}{k\,\theta} \\ 0 & -\mathcal{R}_c & 0 \\ 0 & 0 & -\mathcal{R}_c \end{pmatrix}$$

The NGM technique specifies that the spectral radius of the FV^{-1} matrix is $\mathcal{R}_c$, i.e., $\mathcal{R}_c = \rho\left(FV^{-1}\right)$.

Thus, $\mathcal{R}_c = \rho\left(FV^{-1}\right) = \frac{S^0\,\alpha\,\gamma}{k_2\,k\,\theta} + \frac{S^0\,\psi}{N^0\,k_2}$

$$\mathcal{R}_c = \frac{\alpha\,\gamma\,\Lambda\,k_5}{(k_1\,k_5 - a_2\,b)\;k_2\,k\,\theta} + \frac{\psi\,\mu\,k\,\theta\,k_5}{(k_1\,k_5 - a_2\,b)\;k_2\,k\,\theta} \;= \frac{(\alpha\,\gamma\,\Lambda + \psi\,\mu\,k\,\theta)\;k_5}{(k_1\,k_5 - a_2\,b)\;k_2\,k\,\theta}. \tag{7}$$

with $k_1 = b + \mu$; $k_2 = c + d_1 + \mu$; $k_5 = a_2 + \mu$ and $\mathcal{S}^0 = \dfrac{\Lambda\, k_5}{k_1\, k_5 - b\, a_2}$; $N^0 = \dfrac{\Lambda}{\mu}$.

Theorem 1 ([29, 30])**.** *The Cholera-free equilibrium point ξ^0 is globally asymptotically stable if and only if $\mathcal{R}_c^{\chi} < 1$, and unstable if $\mathcal{R}_c^{\chi} \geq 1$, where $\chi \in (0, 1]$.*

Proof. The system (3) at cholera-free equilibrium ξ^0 has the following Jacobian matrix,

$$J(\xi^0) = \begin{pmatrix} -k_1 & -\frac{k_5\mu\psi}{k_6} & 0 & a_1 & a_2 & -\frac{k_5\Lambda\alpha}{k_6 k} \\ 0 & \frac{k_5\mu\psi}{k_6} - k_2 & 0 & 0 & 0 & \frac{k_5\Lambda\alpha}{k_6 k} \\ 0 & c & -k_3 & 0 & 0 & 0 \\ 0 & 0 & e & -k_4 & 0 & 0 \\ b & 0 & 0 & 0 & -k_5 & 0 \\ 0 & \gamma & 0 & 0 & 0 & -\theta \end{pmatrix}.$$

with the following characteristic polynomial:

$$\mathcal{P}_J(\lambda) = (\lambda + k_3)(\lambda + k_4) \times [\lambda^2 + \lambda(k_1 + k_5) + \overbrace{k_1 k_5 - a_2 b}^{>0}] \times [A_2\lambda^2 + A_1\lambda + A_0],$$

with $A_2 = k(k_1 k_5 - a_2 b) > 0$, $A_1 = k(k_1 k_5 - a_2 b)(\theta + k_2)(1 - \frac{k_5\mu\psi}{(k_1 k_5 - a_2 b)(\theta + k_2)})$, and $A_0 = k k_2 (k_1 k_5 - a_2 b)(1 - \mathcal{R}_c)$.

Note that A_0 is positive iff $\mathcal{R}_c < 1$. It then follows that the characteristic polynomial has all its solutions with negative real part, which means that solutions of the following equation

$$\left(s\left[I_6 - (1-\chi)J(\xi^0)\right] - \chi J(\xi^0)\right) = 0$$

have negative real parts [31, 32]. Now, it remains to prove the possibility that the CFE is globally asymptotically stable. The study of global stability at Cholera-free equilibrium is important to assess whether control measures put in place are effective in eliminating the disease. This makes it possible to predict whether the disease may return after eradication, and to identify long-term monitoring strategies.

We proceed as in [33, Theorem 2.1]. For this aim, let $f = (\mathcal{S}, \mathcal{I}, \mathcal{T}, \mathcal{R}, \mathcal{V}, \mathcal{B})^T$ and $g = (\mathcal{I}, \mathcal{T}, \mathcal{B})^T$. From (3), we have:

$${}_0^C\mathcal{D}_t^{\chi} g = (F + V)g - \mathcal{M}(\mathcal{S}, \mathcal{I}, \mathcal{T}, \mathcal{R}, \mathcal{V}, \mathcal{B}),$$

where F and V are given by F(x) and V(x) respectively, and

$$\mathcal{M}(\mathcal{S},\mathcal{I},\mathcal{T},\mathcal{R},\mathcal{V},\mathcal{B}) = \begin{pmatrix} \mathcal{N}(\mathcal{S},\mathcal{I},\mathcal{T},\mathcal{R},\mathcal{V},\mathcal{B}) \\ 0 \\ 0 \end{pmatrix},$$

where $\mathcal{N}(\mathcal{S},\mathcal{I},\mathcal{T},\mathcal{R},\mathcal{V},\mathcal{B}) = \mathcal{S}_0\left[\left(1-\alpha\frac{\mathcal{B}}{k+\mathcal{B}}.\frac{\mathcal{S}}{\mathcal{S}_0}\right)+\left(1-\psi\frac{\mathcal{I}}{N}.\frac{\mathcal{S}}{\mathcal{S}_0}\right)\right] \geq 0,\ \forall t > 0$. Then, it follows that $\mathcal{M}(\mathcal{S},\mathcal{I},\mathcal{T},\mathcal{R},\mathcal{V},\mathcal{B}) \geq \mathbf{O}_{\mathbb{R}^3}$, which implies that ${}_0^C\mathcal{D}_t^{\chi} g \leq (F+V)g$.

Note that the eigenvalues of $J(\xi^0) = F+V$ contain negative real components. ξ^0 is stable if $\mathcal{R}_c < 1$. This implies that $g \to \mathbf{O}_{\mathbb{R}^3}$ as $t \to \infty$. Furthermore, $F \geq \mathbf{O}_{\mathbb{R}^{3\times 3}}$. and $-V^{-1} > \mathbf{O}_{\mathbb{R}^{3\times 3}}$. According to [33, Theorem 2.1], there exists a Lyapunov function $\mathcal{L} = q(-V^{-1})g$ where q represents the left eigenvector of $-V^{-1}F$, corresponding to the eigenvalue $\mathcal{R}_c$. Then, ${}_0^C\mathcal{D}_t^{\chi}\mathcal{L} = (\mathcal{R}_c - 1)qg - q(-V^{-1})\mathcal{M} \leq 0$. It follows that $\left\{\xi^0\right\}$. is the largest invariant set that contains $\left\{\lambda \in \mathbb{R}^5 :{}_0^C\ \mathcal{D}_t^{\chi}\mathcal{L} = 0\right\}$. The global stability of ξ^0 is determined by the LaSalle Invariance Principle [34]. This ends the proof. □

3.3.2 Existence of the Cholera-endemic equilibrium points

Here, we will prove the existence of at least one Cholera-endemic equilibrium point. To this aim, let define by $\zeta^* = (\mathcal{S}^*,\mathcal{I}^*,\mathcal{T}^*,\mathcal{R}^*,\mathcal{V}^*,\mathcal{B}^*)$ any equilibrium of our system (3).

At endemic equilibrium state, the FOI become $\varphi_1^* = \alpha\frac{B^*}{k+B^*}$ and $\varphi_2^* = \psi\frac{\mathcal{I}^*}{N^*}$, where $N^* = \frac{\Lambda - d_1\mathcal{I}^* - d_2\mathcal{T}^*}{\mu}$. By setting the right-hand side of system (3) (with $\chi = 1$) equal to zero and expressing the state variables in term of φ_1^* and φ_2^* , the components of any equilibrium point ζ^* are given by:

$$\mathcal{S}^* = \frac{k_2\mathcal{I}^*}{\varphi_1^*+\varphi_2^*}, \mathcal{V}^* = \frac{b\mathcal{S}^*}{k_5}, \mathcal{T}^* = \frac{c\mathcal{I}^*}{k_3}, \mathcal{R}^* = \frac{e\mathcal{T}^*}{k_4}, \mathcal{B}^* = \frac{\gamma\mathcal{I}^*}{\theta}, \tag{8}$$

where I^* is the nonnegative solutions of the following equation

$$\left[A_2(\mathcal{I}^*)^2 + A_1\mathcal{I}^* + A_0\right]\mathcal{I}^* = 0, \tag{9}$$

with

$$A_2 = \mathcal{R}_c(k_2k_3k_4 - a_1ce)k\gamma\theta(k_3\mu\psi - (d_2c+d_1k_3)\alpha) - k_3k_4\gamma(d_2c+d_1k_3)(k\theta\mu\psi + \Lambda\alpha\gamma),$$

$$\begin{aligned} A_1 = &\left(\left(-\mathcal{R}_ca_1k_3ce - d_2k_3k_4c + (\mathcal{R}_ck_2 - d_1){k_3}^2k_4\right)k^2\theta^2 + (1-\mathcal{R}_c){k_3}^2k_4k\Lambda\gamma\theta\right)\mu\psi \\ &+ \left(-\mathcal{R}_ca_1k_3ce + (\mathcal{R}_c-1)d_2k_3k_4c + (\mathcal{R}_ck_2 + (\mathcal{R}_c-1)d_1){k_3}^2k_4\right)k\Lambda\alpha\gamma\theta + {k_3}^2k_4\Lambda^2\alpha\gamma^2, \end{aligned}$$

$$A_0 = -\left(\mathcal{R}_c - 1\right) {k_3}^2 k_4 k \Lambda \theta \left(k\theta\mu\psi + \Lambda\alpha\gamma\right),$$

It is clear that $A_0 < 0$ if $\mathcal{R}_c > 1$. Thus, using Descartes rule of sign, we therefore conclude that model (3) can admits 0, 1 or 2 endemic equilibrium points if only if $\mathcal{R}_c > 1$ (respectively $\mathcal{R}_c < 1$). We thus claim what follows:

Theorem 2. *Model* (3) *admits at least one Cholera-endemic equilibrium point whenever* $\mathcal{R}_c > 1$. *If* $\mathcal{R}_c < 1$, *and depending on the sign of coefficient* A_2 *and* A_1, *there is a possibility that the Cholera-free equilibrium coexists with two endemic equilibrium points.*

3.4 Numerical scheme

In this section, we develop the numerical technique required to simulate our fractional model. Numerical algorithms are essential for approximating the solutions of nonlinear ordinary and partial differential equations that cannot be solved through standard analytical approaches. Several methods have been proposed for solving fractional differential equations, including Euler's method, the Adams–Bashforth–Moulton method, the Adomian Decomposition method, the Homotopy Analysis method, the Laplace–Adomian Decomposition method, and the Polynomial Interpolation method [11, 17, 35]. Among these, we select the Adams–Bashforth–Moulton method because of its stability and efficiency [36, 37]. Accordingly, we apply this method to our model.

By considering the following fractional differential equation

$$\begin{cases} {}^{C}\mathcal{D}_t^{\chi} f(t) = k(t, q(t)), & 0 \leq t \leq T \\ q^g(0) = q_0^g, & g = 0, 1, 2..., -1 + m, \end{cases} \tag{10}$$

where $m = [\chi]$.

It corresponds to the following Voltera integral equation:

$$q(t) = \sum_{\dot{g}=0}^{-1+m} q^g \frac{t^g}{g!} + \frac{1}{\Gamma(\chi)} \int_0^t (t - \varphi)^{\chi - 1} q(\varphi, k(\varphi)) d\varphi. \tag{11}$$

Using the Diethelm and Neville technique [38] and the Adams-Bashforth-Moulton algorithm [39], the numerical scheme for the fractional Cholera model (3) is as follows:

Let $0 < \chi \leq 1$, $t \in [0; T]$, $q = \dfrac{T}{m}$, $t_n = n.q$, $n = 0, 1, 2..., m \in \mathbb{N}$. The solution of (3) is given by

$$\begin{cases}
\mathcal{S}_{n+1} = \mathcal{S}_0 + \dfrac{q^\chi}{\Gamma(\chi+2)}(\Lambda - \left(\dfrac{\alpha\,\mathcal{B}_{n+1}}{k+\mathcal{B}_{n+1}} + \psi\,\dfrac{\mathcal{I}_{n+1}}{N}\right)\mathcal{S}_{n+1} + a_1\,\mathcal{R}_{n+1} + a_2\,\mathcal{V}_{n+1} - (b+\mu)\mathcal{S}_{n+1}) \\
\qquad + \dfrac{q^\chi}{\Gamma(\chi+2)}\displaystyle\sum_{j=0}^{n} a_{j,n+1}(\Lambda - \left(\dfrac{\alpha\,\mathcal{B}_j}{k+\mathcal{B}_j} + \psi\,\dfrac{\mathcal{I}_j}{N}\right)\mathcal{S}_j + a_1\,\mathcal{R}_j + a_2\,\mathcal{V}_j - (b+\mu)\mathcal{S}_j), \\
\mathcal{I}_{n+1} = \mathcal{I}_0 + \dfrac{q^\alpha}{\Gamma(\chi+2)}(\left(\dfrac{\alpha\,\mathcal{B}_{n+1}}{k+\mathcal{B}_{n+1}} + \psi\,\dfrac{\mathcal{I}_{n+1}}{N}\right)\mathcal{S}_{n+1} - (c+d_1+\mu)\mathcal{I}_{n+1}) \\
\qquad + \dfrac{q^\chi}{\Gamma(\chi+2)}\displaystyle\sum_{j=0}^{n} a_{j,n+1}(\left(\dfrac{\alpha\,\mathcal{B}_j}{k+\mathcal{B}_j} + \psi\,\dfrac{\mathcal{I}_j}{N}\right)\mathcal{S}_j - (c+d_1+\mu)\mathcal{I}_j), \\
\mathcal{T}_{n+1} = \mathcal{T}_0 + \dfrac{q^\chi}{\Gamma(\chi+2)}(c\mathcal{I}_{n+1} - (e+d_2+\mu)\mathcal{T}_{n+1}) + \dfrac{q^\chi}{\Gamma(\chi+2)}\displaystyle\sum_{j=0}^{n} a_{j,n+1}(c\mathcal{I}_j - (e+d_2+\mu)\mathcal{T}_j), \\
\mathcal{R}_{n+1} = \mathcal{R}_c + \dfrac{q^\chi}{\Gamma(\chi+2)}(e\,\mathcal{T}_{n+1} - (a_1+\mu)\mathcal{R}_{n+1}) + \dfrac{q^\chi}{\Gamma(\chi+2)}\displaystyle\sum_{j=0}^{n} a_{j,n+1}(e\,\mathcal{T}_j - (a_1+\mu)\mathcal{R}_j), \\
\mathcal{V}_{n+1} = \mathcal{V}_0 + \dfrac{q^\chi}{\Gamma(\chi+2)}(b\,\mathcal{S}_{n+1} - (a_2+\mu)\mathcal{R}_{n+1}) + \dfrac{q^\chi}{\Gamma(\chi+2)}\displaystyle\sum_{j=0}^{n} a_{j,n+1}(b\,\mathcal{S}_j - (a_2+\mu)\mathcal{V}_j), \\
\mathcal{B}_{n+1} = \mathcal{B}_0 + \dfrac{q^\chi}{\Gamma(\chi+2)}(\gamma\,\mathcal{I}_{n+1} - \theta\,\mathcal{B}_{n+1}) + \dfrac{q^\chi}{\Gamma(\chi+2)}\displaystyle\sum_{j=0}^{n} a_{j,n+1}(\gamma\,\mathcal{I}_j - \theta\,\mathcal{B}_j),
\end{cases} \tag{12}$$

where

$$\begin{aligned}
\mathcal{S}^p_{n+1} &= \mathcal{S}_0 + \frac{1}{\Gamma(\chi)}\sum_{j=0}^{n} b_{j,n+1}(\Lambda - \left(\frac{\alpha\,\mathcal{B}_j}{k+\mathcal{B}_j} + \psi\,\frac{\mathcal{I}_j}{N}\right)\mathcal{S}_j + a_1\,\mathcal{R}_j + a_2\,\mathcal{V}_j - (b+\mu)\mathcal{S}_j), \\
\mathcal{I}^p_{n+1} &= \mathcal{I}_0 + \frac{1}{\Gamma(\chi)}\sum_{j=0}^{n} b_{j,n+1}(\left(\frac{\alpha\,\mathcal{B}_j}{k+\mathcal{B}_j} + \psi\,\frac{\mathcal{I}_j}{N}\right)\mathcal{S}_j - (c+d_1+\mu)\mathcal{I}_j), \\
\mathcal{T}^p_{n+1} &= \mathcal{T}_0 + \frac{1}{\Gamma(\chi)}\sum_{j=0}^{n} b_{j,n+1}(c\mathcal{I}_j - (e+d_2+\mu)\mathcal{T}_j), \\
\mathcal{R}^p_{n+1} &= \mathcal{R}_c + \frac{1}{\Gamma(\chi)}\sum_{j=0}^{n} b_{j,n+1}(e\,\mathcal{T}_j - (a_1+\mu)\mathcal{R}_j), \\
\mathcal{V}^p_{n+1} &= \mathcal{V}_0 + \frac{1}{\Gamma(\chi)}\sum_{j=0}^{n} b_{j,n+1}(b\,\mathcal{S}_j - (a_2+\mu)\mathcal{V}_j), \\
\mathcal{B}^p_{n+1} &= \mathcal{B}_0 + \frac{1}{\Gamma(\chi)}\sum_{j=0}^{n} b_{j,n+1}(\gamma\,\mathcal{I}_j - \theta\,\mathcal{B}_j),
\end{aligned} \tag{13}$$

and

$$a_{j,1+n} = \begin{cases}
n^{1+p} - (-\chi+n)(1+n), & if \quad j = 0, \\
(2+n-j)^{1+\chi} - 2(n+1-j)^{1+\chi} + (-j+n)^{1+\chi}, & if \quad 1 \leq j \leq n, \\
1, & if \quad j = 1+n.
\end{cases}$$

$$b_{j,1+n} = \frac{q^\chi}{\chi}((1+n-j)^\chi - (-j+n)^\chi), \quad 0 \leq j \leq n.$$

The convergence and precision of this scheme can be found in [39] (see also [40, 41]).

3.5 Data information, Parameters estimation and, Forecasting

The study focuses on Cameroon, a Central African country located on the Gulf of Guinea. Covering a total area of 475, 650 square kilometers, it has a trapezoidal shape and shares borders with Nigeria, Congo, Gabon, Equatorial Guinea, the Central African Republic, and Chad.

Cameroon's diverse natural environment comprises ten regions, earning it the nickname "Africa in miniature," as it reflects much of the continent's geographic and ecological variety. In recent years, cholera has become endemic in the Cameroonian population. Between epidemiological weeks 22 of 2022 and 09 of 2023, the disease was reported in eight regions of the country: Centre, East, Far North, Littoral, North, West, South, and South-West. Among these, the Littoral region was the most severely affected. This can be attributed to its varied relief, which includes the coastal plain and the Wouri estuary, plateaus and hills, as well as mountainous and volcanic areas. The region's hydrographic network is dense and intertwined, influenced by high humidity and the impermeability of its crystalline soil formations. All rivers in this region drain into the Atlantic basin and are subject to an equatorial climate. Due to the abundance of water in the soil, *Vibrio cholerae* thrives particularly well in this environment.

Figure 3 shows the cholera cases reported in eight (08) regions of Cameroon during the period from week 22 of 2022 to week 9 of 2023[2]. To this aim, we take into account data from this region of Cameroon during the period

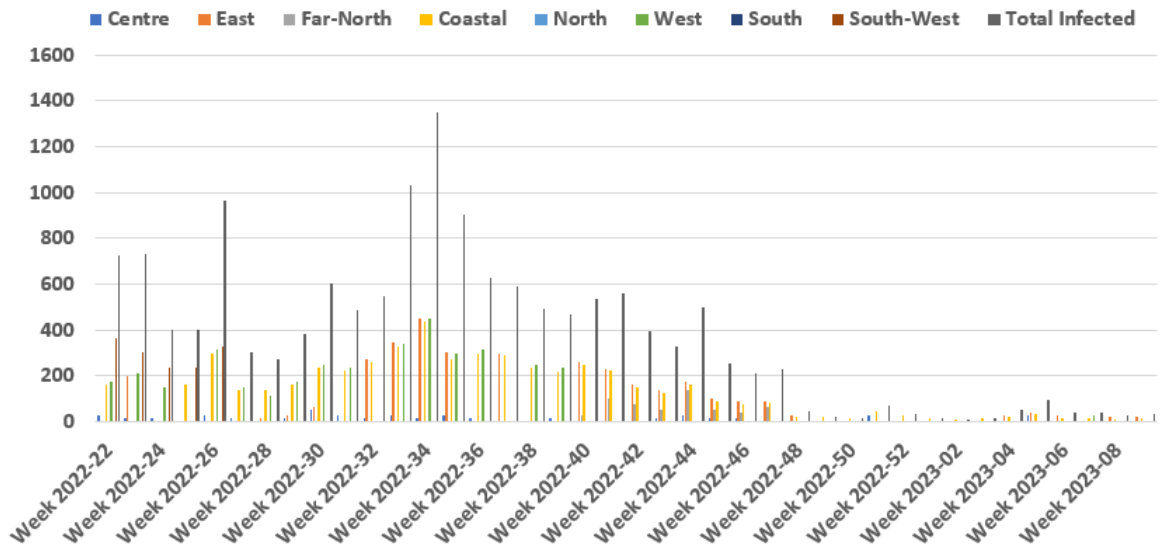

Figure 3: Histogram of the Cholera epidemic evolution by region in Cameroon during the period from week 22 of 2022 to week 9 of 2023.

from week 2022-22 to week 2023-09 to calibrate our cholera model (3).

We wish to demonstrate the importance of using the fractional derivative rather than the integer derivative. To

[2] http://www.ccousp.cm/documentations/rapports-de-situation

do this, we'll compute the root mean square error (RMSE), which is a commonly used measure of the discrepancies between the values predicted by a model or estimator and the observed values (or real values). The expression is as follows:

$$RMSE = \sqrt{\sum_{i=1}^{n} \frac{1}{n} \left(X_i - \overline{X}_i\right)^2}. \tag{14}$$

where n is size of the dataset, X_i and $\overline{X}_i$ are the number of detected cases and predicted cases at the time t_i, respectively. The results of model calibration are listed in figure 4 and table 2.

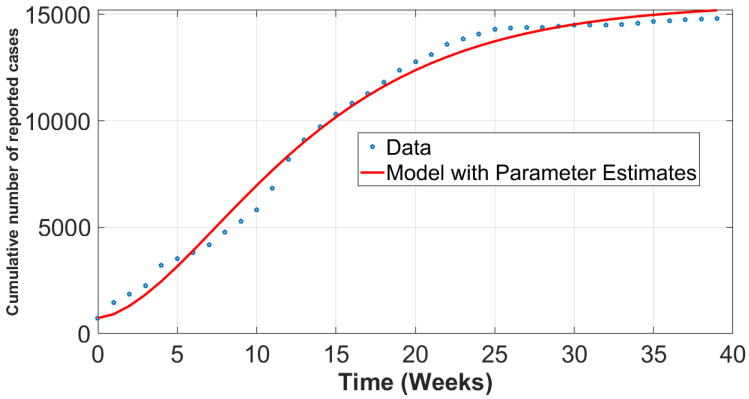

Figure 4: Cumulative Cholera cases in Cameroon versus model simulation.

Table 2: Values of fitted parameters with $\mathcal{R}_c = 2.0439$ when $\chi = 1$. $\star$ refers to https://www.imf.org/external/pubs/ft/fabric/fra/camprof.htm

Parameters	Values	Source	Parameters	Values	Source
Λ	$\mu * N_0$	Estimated	c	0.1228	Fitted
μ	$1/(52 * 56)$	$\star$	e	0.0902	Fitted
α	3.4938×10^{-8}	Fitted	d_1	6.2289×10^{-4}	Fitted
k	196.1808	Fitted	d_2	9.3140×10^{-4}	Fitted
a_1	0.8973	Fitted	γ	1.0427	Fitted
a_2	0.6236	Fitted	ψ	0.0228	Fitted
b	0.5245	Fitted	θ	0.0126	Fitted

Note that $\mathcal{R}_c = 2,0439$ means that the disease is endemic in the country since $\mathcal{R}_c > 1$. This suggests that many efforts must be made by health authorities to stop the spread of this disease.

To compare the model formulated with classical-order derivative ($\chi = 1$) and the one formulated with fractional-order derivative ($0 < \chi < 1$), we use, as metric, the root means square error defined by equation (14). The smaller RMSE means that the corresponding model is better adapter to predict the disease dynamics in the country. We thus obtain results displayed in table 3.

Table 3: Root Means Square Error (RMSE) of different fractional-order values and the corresponding value of $\mathcal{R}_c$.

χ	1	0.91	0.90
$RMSE$	67789.02	67773.58	67767.54
$\mathcal{R}_c$	2.0439	1.1793	1.1121

From table 3, it follows that for the fractional order $\chi = 1$, the corresponding RMSE is equal to 67789.02, while for $\chi = 0.91$ and $\chi = 0.90$, the corresponding RMSE are equal to 67773.58 and 67767.54, respectively. We can therefore conclude that the fractional model is better suited than the classical model (ODE). This is also illustrated in figure 5.

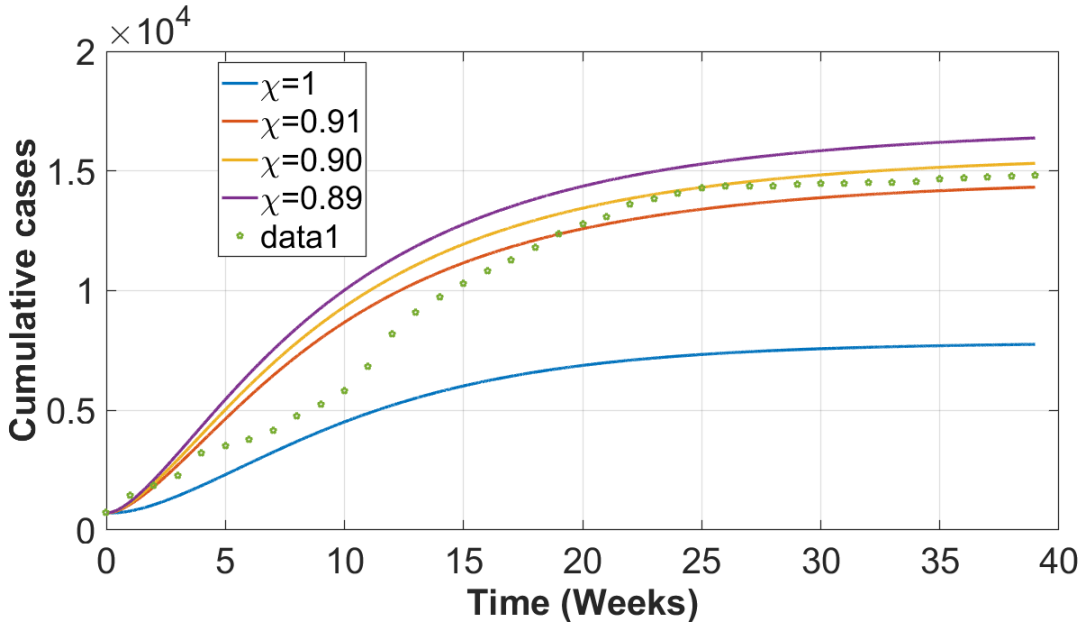

Figure 5: Cumulative cholera cases in Cameroon from weekends $2022-22$ to $2023-09$ versus model predictions with different fractional-order χ values.

The graph presented in figure 6 suggests that peak in the total number of cumulative cases is reached as early as week 3, followed by a gradual decline until week 110, after which it stabilizes until week 216. These observation could reflect the effectiveness of the measures put in place by the authorities of country to contain and eradicate this epidemic.

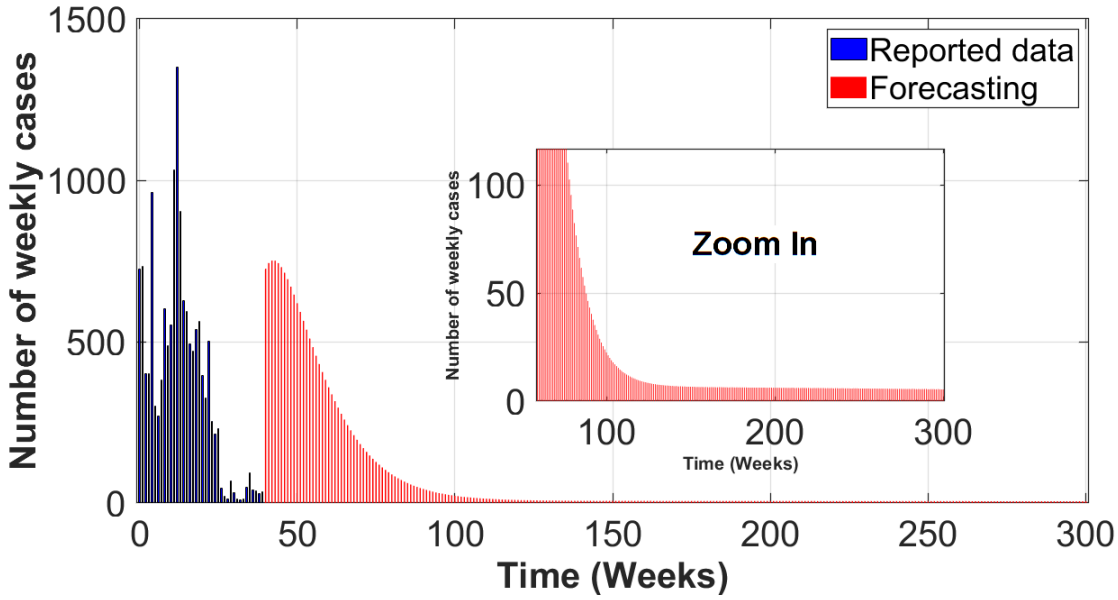

Figure 6: Forecasting a new Cholera cases in Cameroon for the next 261 weeks, i.e, from the week of $2023-09$ to the week of $2027-10$. In other words, a prediction over 05 years and one week.

3.6 Sensitivity analysis

Here, we use sensitivity analysis to discover which model parameter is the most important in disease dynamics. To do this, we follow Chitnis et *al.* [42] and calculate the sensitivity index for each model parameter that appears in the equation of $\mathcal{R}_c$. The following formula calculates the sensitivity index for each model parameter, represented by Θ:

$$\Pi_\Theta := \frac{\Theta}{\mathcal{R}_c}\frac{\partial \mathcal{R}_c}{\partial \Theta}. \tag{15}$$

The sensitivity of $\mathcal{R}_c$ to parameter changes is indicated by this index. It is evident that a positive (or negative) index means that a rise in the parameter value causes the $\mathcal{R}_c$ value to rise (or fall) [42]. For example, the sensitivity index of $\mathcal{R}_c$ with regard to ψ can be calculated as follows:

$$\Pi_\psi := \frac{\psi}{\mathcal{R}_c}\frac{\partial \mathcal{R}_c}{\partial \psi} = \frac{k\mu\psi\theta}{\Lambda\alpha\gamma + k\mu\psi\theta} > 0.$$

This demonstrates that the parameter ψ affects the spread of sickness and that $\mathcal{R}_c$ is an increasing function of ψ, while for c, we have

$$\mathcal{S}_c^{\mathcal{R}_c} = -\frac{c}{\mu + d_1 + c} < 0,$$

which prove that the parameter c affects the spread of sickness and that $\mathcal{R}_c$ is an decreasing function of c. For the other parameters, we have:

$$
\begin{aligned}
\mathcal{S}_{\Lambda}^{\mathcal{R}_c} =& \frac{\Lambda\alpha\gamma}{\Lambda\alpha\gamma + k\mu\psi\theta} > 0, \quad \mathcal{S}_{\alpha}^{\mathcal{R}_c} = \frac{\Lambda\alpha\gamma}{\Lambda\alpha\gamma + k\mu\psi\theta} > 0, \quad \mathcal{S}_{\gamma}^{\mathcal{R}_c} = \frac{\Lambda\alpha\gamma}{\Lambda\alpha\gamma + k\mu\psi\theta} > 0, \\
\mathcal{S}_{\mu}^{\mathcal{R}_c} =& \frac{1}{(\mu + a_2)(\Lambda\alpha\gamma + k\mu\psi\theta)} \times \\
& \times \{k\mu(\mu + d_1 + c)((\mu + a_2)(\mu + b) - a_2 b)\theta \times \\
& \times \left(\frac{\Lambda\alpha\gamma + k\mu\psi\theta}{k(\mu + d_1 + c)((\mu + a_2)(\mu + b) - a_2 b)\theta} - \frac{(\mu + a_2)(\Lambda\alpha\gamma + k\mu\psi\theta)}{k(\mu + d_1 + c)^2((\mu + a_2)(\mu + b) - a_2 b)\theta} \right. \\
& \left. - \frac{(\mu + a_2)(2\mu + b + a_2)(\Lambda\alpha\gamma + k\mu\psi\theta)}{k(\mu + d_1 + c)((\mu + a_2)(\mu + b) - a_2 b)^2\theta} + \frac{(\mu + *_2)\psi}{(\mu + d_1 + c)((\mu + a_2)(\mu + b) - a_2 b)} \right) \Big\}, \\
\mathcal{S}_{d_1}^{\mathcal{R}_c} =& -\frac{d_1}{\mu + d_1 + c} < 0, \\
\mathcal{S}_{a_2}^{\mathcal{R}_c} =& \frac{a_2 k(\mu + d_1 + c)((\mu + a_2)(\mu + b) - a_2 b)\theta}{(\mu + a_2)(\Lambda\alpha\gamma + k\mu\psi\theta)} \times \\
& \times \left(\frac{\Lambda\alpha\gamma + k\mu\psi\theta}{k(\mu + d_1 + c)((\mu + a_2)(\mu + b) - a_2 b)\theta} - \frac{\mu(\mu + a_2)(\Lambda\alpha\gamma + k\mu\psi\theta)}{k(\mu + d_1 + c)((\mu + a_2)(\mu + b) - a_2 b)^2\theta} \right), \\
\mathcal{S}_{b}^{\mathcal{R}_c} =& -\frac{b\mu}{(\mu + a_2)(\mu + b) - a_2 b} < 0,
\end{aligned}
$$

$$
\begin{aligned}
\mathcal{S}_{k}^{\mathcal{R}_c} =& \frac{k^2(\mu + d_1 + c)((\mu + a_2)(\mu + b) - a_2 b)\theta}{(\mu + a_2)(\Lambda\alpha\gamma + k\mu\psi\theta)} \times \\
& \times \left\{ \frac{\mu(\mu + a_2)\psi}{k(\mu + d_1 + c)((\mu + a_2)(\mu + b) - a_2 b)} - \frac{(\mu + a_2)(\Lambda\alpha\gamma + k\mu\psi\theta)}{k^2(\mu + d_1 + c)((\mu + a_2)(\mu + b) - a_2 b)\theta} \right\}, \\
\mathcal{S}_{\theta}^{\mathcal{R}_c} =& \frac{k(\mu + d_1 + c)((\mu + a_2)(\mu + b) - a_2 b)\theta^2}{(\mu + a_2)(\Lambda\alpha\gamma + k\mu\psi\theta)} \times \\
& \times \left(\frac{\mu(\mu + a_2)\psi}{(\mu + d_1 + c)((\mu + a_2)(\mu + b) - a_2 b)\theta} - \frac{(\mu + a_2)(\Lambda\alpha\gamma + k\mu\psi\theta)}{k(\mu + d_1 + c)((\mu + a_2)(\mu + b) - a_2 b)\theta^2} \right).
\end{aligned}
$$

Consider the sign of $\mathcal{S}_{\mu}^{\mathcal{R}_c}$., $\mathcal{S}_{a_2}^{\mathcal{R}_c}$., $\mathcal{S}_{k}^{\mathcal{R}_c}$, and $\mathcal{S}_{\theta}^{\mathcal{R}_c}$ depends of parameter values.

Figure 7 displays the sensitivity level of each model parameter.

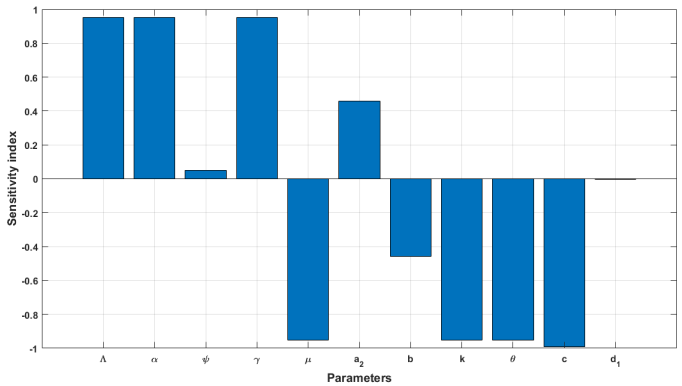

Figure 7: Sensitivity indices for $\mathcal{R}_c$ against model parameters.

The impact of vaccine coverage b and bacterial decay rate θ on the disease dynamics is depicted on figure 8. We

clearly see that the increase of vaccination coverage combined with the decrease of the bacterial in environment can have a great impact on the reduction of the number of infected cases.

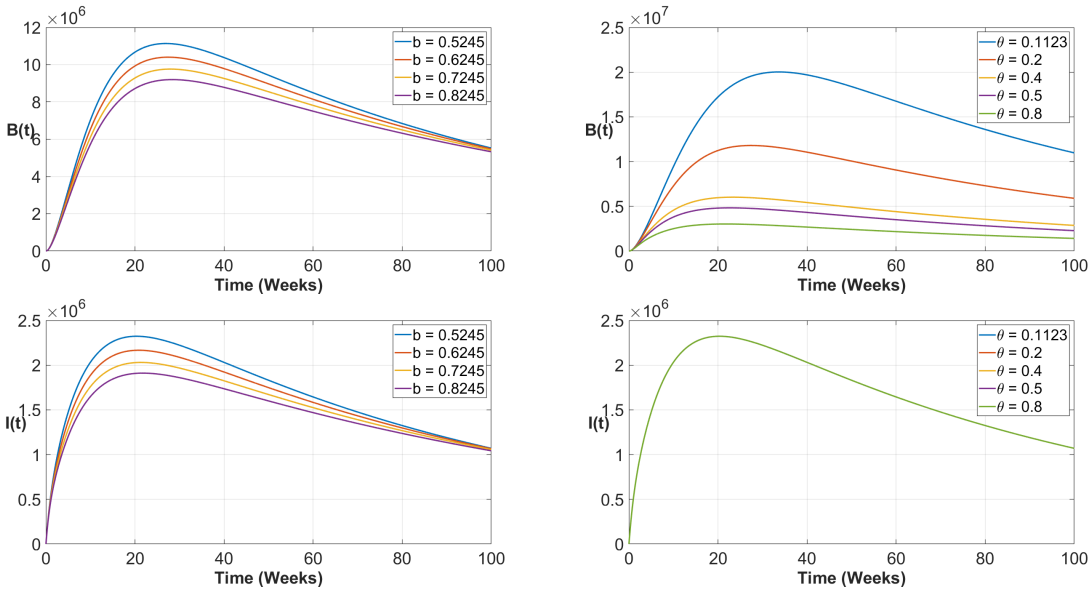

Figure 8: Impact of vaccine coverage and bacterial decay rate on the disease dynamics.

3.7 Numerical results of our model equations

In this part, we use the numerical scheme mentioned above to simulate the fractional model (3).

3.7.1 The autonomous model

In this section, we present the numerical solutions. For the simulations, we use the parameter values listed in Table 2, where all values are expressed in $week^{-1}$, except for the contribution of infected populations to bacterial concentration, which occurs at rate γ expressed in $cell/\left(ml \cdot week \cdot person\right)$, and the half-saturation constant k, expressed in $cell/ml$. The results are illustrated in Figures 9 and 10. The findings show that when $\mathcal{R}_c$ is less than one, the number of infected individuals tends to zero, whereas the system converges to an endemic equilibrium when $\mathcal{R}_c$ is greater than one. In both scenarios, the concentration of free bacteria in the environment increases, highlighting the necessity of sustained efforts to eliminate free-living bacteria. Effective control of cholera therefore requires not only rapid treatment of patients but also the implementation of policies aimed at raising public awareness about the harmful effects of the disease and the importance of maintaining hygienic living conditions.

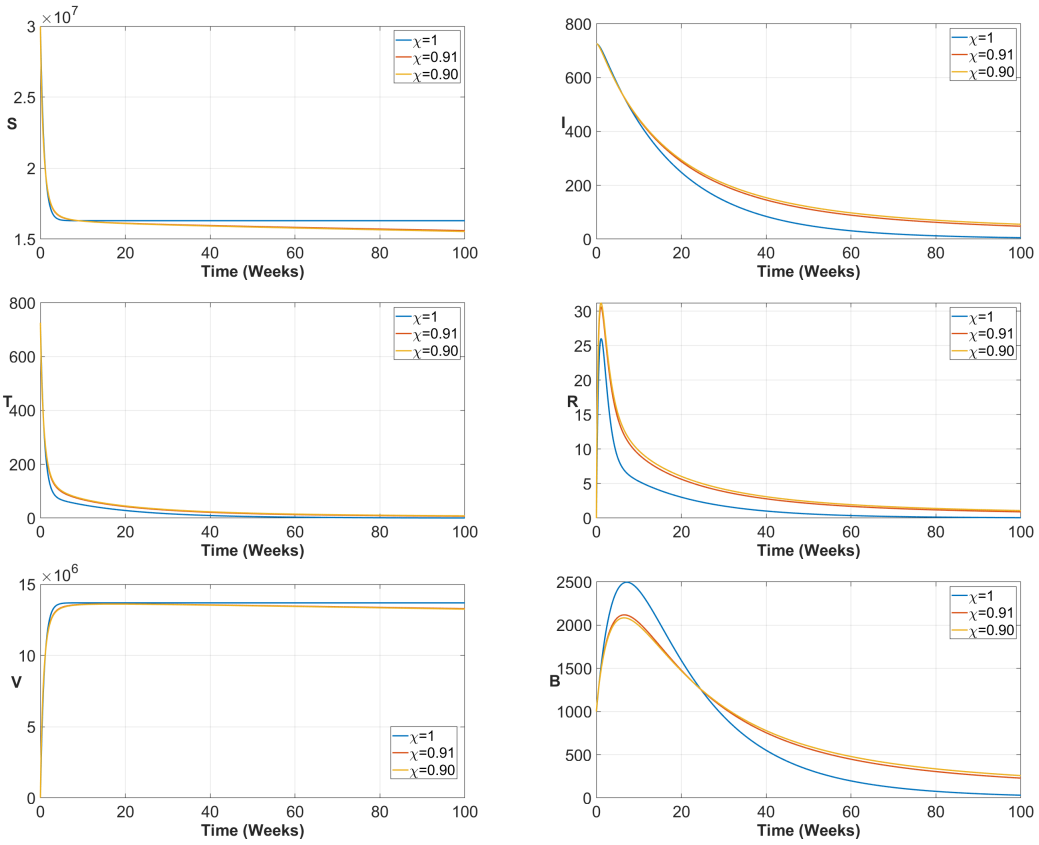

Figure 9: Time-series of fractional model (3) showing the impact of varying the fractional-order $\chi \in \{1, 0.91, 0.90\}$ at the Cholera-free equilibrium.

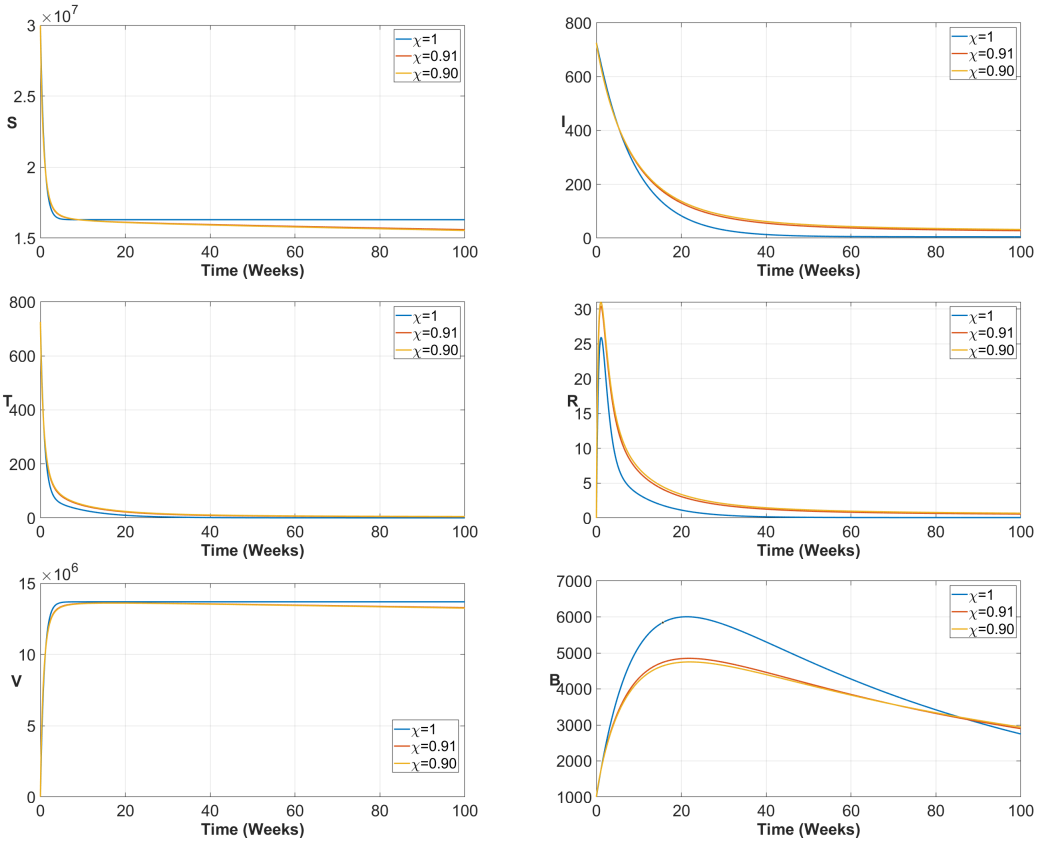

Figure 10: Time-series of fractional model (3) showing the impact of varying the fractional-order $\chi \in \{1; 0.95; 0.90\}$ at the Cholera-endemic equilibrium.

3.7.2 The non-autonomous model

In this part, we consider the time varying transmission rates follow the equations:

$$\begin{cases} \psi(t) & := \psi_0 \left(1 + \omega_1 \cos\left(\dfrac{2\pi t}{52} + \omega_2\right)\right) \\ \alpha(t) & := \alpha_0 \left(1 + \omega_1 \cos\left(\dfrac{2\pi t}{52} + \omega_2\right)\right) \end{cases} \tag{16}$$

where $\psi_0 = 3.4938 \times 10^{-8}$ (resp. $\alpha_0 = 0.0228$), $\omega_1 = 1$, and $\omega_2 = \dfrac{\pi}{26}$ denote the baseline transmission rate for Cholera from infectious human (resp. from free bacteria), the magnitude of the forcing, and the initial phase, respectively. The results are displayed on figures 11 and 12. This demonstrates the persistence of the disease and the existence of periodic solutions.

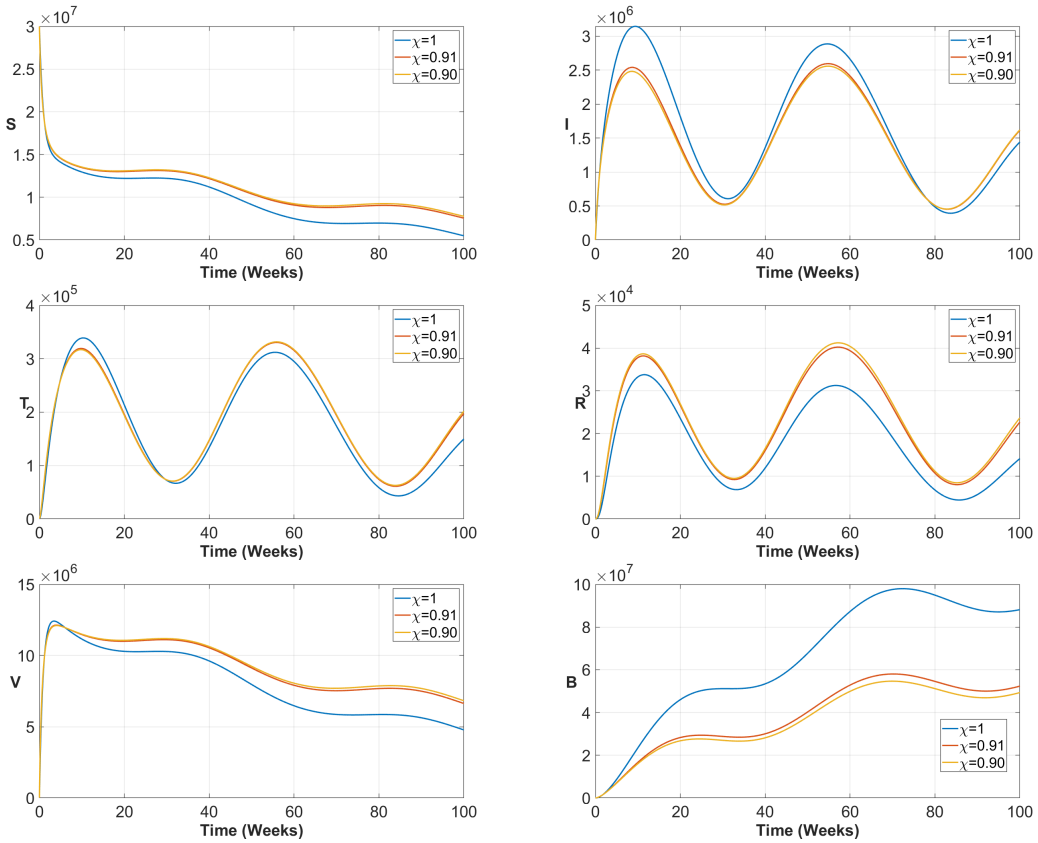

Figure 11: Persistence of the disease when $\mathcal{R}_c = 2.0439 > 1$, given the specific parameter values specified in Table 2.

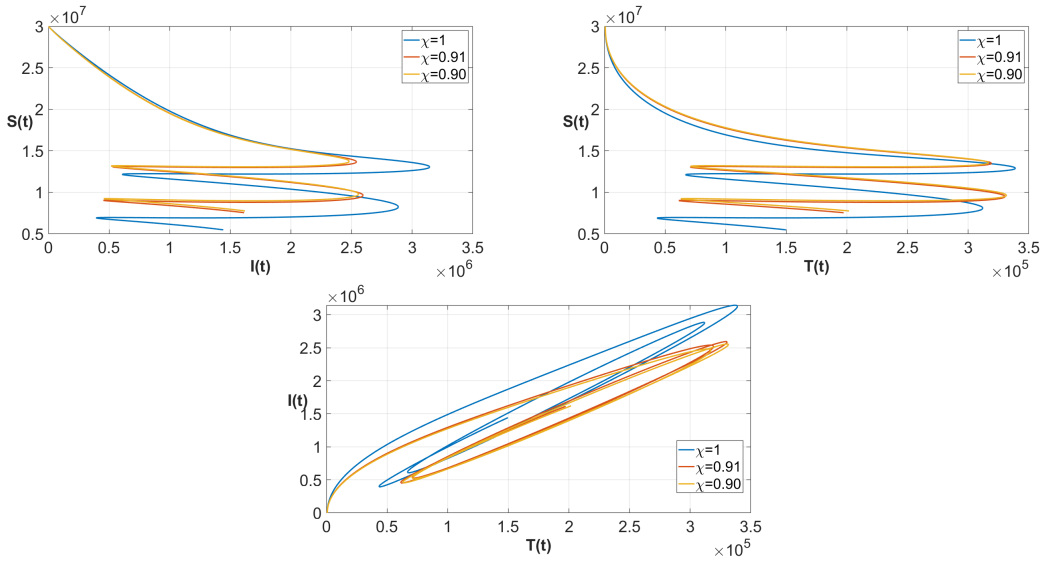

Figure 12: Periodic solutions of the disease when $\mathcal{R}_c = 2.0439 > 1$, given the specific parameter values specified in Table 2.

4 Discussions

In this section, we examine in detail the impact of seasonal changes in Cameroon on the evolution of cholera cases. Like many other countries, Cameroon experiences two distinct seasons: the dry season and the rainy season, each lasting approximately six months. The transition between these seasons plays a crucial role in shaping the dynamics of cholera incidence in the country.

During the dry season, the limited availability of water restricts the development of the pathogenic *Vibrio cholerae* bacterium, which is typically transmitted through contaminated water and food. By contrast, the rainy season—particularly in the coastal region, where the majority of cases are reported—is associated with rising water levels that increase population exposure to cholera risk. Frequent flooding in this region, as well as landslides that are more common in the Western and Central parts of the country, further hinder access to healthcare services for infected individuals.

The results of these observations are illustrated in Figures 11 and 12, which provide a visual overview of the seasonal impact on cholera transmission. The cosine function employed in this section serves as an appropriate mathematical representation of seasonal variation. Meanwhile, Figures 9 and 10 correspond to observations during the dry season, when government-implemented preventive measures appear to be more effective in controlling the epidemic.

This analysis highlights the critical importance of accounting for seasonal variations in understanding the evolution of cholera in Cameroon. It emphasizes the need to adapt prevention and intervention strategies to climatic conditions in order to improve the effectiveness of efforts to combat this devastating infectious disease.

5 Conclusion

The goal of this study was to formulate and analyze a fractional-order model of the transmission dynamics of cholera using real data from Cameroon. To this end, we extended existing work by modifying the force of infection (FOI) and replacing integer-order derivatives with fractional-order derivatives in the Caputo sense.

After formulating the model, we demonstrated the non-negativity and boundedness of solutions, as well as their existence and uniqueness. Using the Next Generation Matrix Method (NGMM), we determined the control reproduction number. With an appropriate Lyapunov function, we showed that the cholera-free equilibrium is globally asymptotically stable whenever the control reproduction number $\mathcal{R}c < 1$. We also established the existence of at least one endemic equilibrium point whenever $\mathcal{R}c > 1$. Several numerical simulations were performed using the Adams–Bashforth–Moulton method to validate our analytical results and to assess the impact of varying the fractional parameter on disease spread. Specifically, when $\mathcal{R}c < 1$, the solutions converge to the cholera-free equilibrium, while for $\mathcal{R}c > 1$, the solutions converge to the endemic equilibrium point. Furthermore, the population of each compartment decreases as the fractional order decreases. We also investigated cases in which the transmission rates ψ and α were time-dependent, and observed disease persistence and the possible existence of periodic solutions.

Sensitivity analysis revealed that the model is highly sensitive to certain parameters. In future work, we plan to extend the model by incorporating temporal control parameters and to apply optimal control theory to identify combinations of interventions capable of rapidly curbing the spread of cholera in Cameroon.

Acknowledgment

The authors thank the Editor and anonymous reviewers for their comments and suggestions that allowed the quality of the work to be improved.

Compliance with Ethical Standards

Author Contribution:

Conceptualization: Rubin Fandio and Hamadjam Abboubakar; **Methodology**: Rubin Fandio, Hamadjam Abboubakar, Sylvain Ardo Gouroudja Banbeto; **Software**: Rubin Fandio, Hamadjam Abboubakar and Sylvain Ardo Gouroudja Banbeto; **Formal analysis**: Rubin Fandio, Hamadjam Abboubakar and Sylvain Ardo Gouroudja Banbeto; **Investigation**: Rubin Fandio, Hamadjam Abboubakar and Sylvain Ardo Gouroudja Banbeto; **Resources**: Hamadjam Abboubakar and Henri Paul Ekobena Fouda; **Data curation**: Rubin Fandio, Hamadjam Abboubakar and Sylvain Ardo Gouroudja Banbeto; **writing—original draft preparation**: Rubin Fandio and Hamadjam

Abboubakar; **Visualization**: Rubin Fandio, Hamadjam Abboubakar and Sylvain Ardo Gouroudja Banbeto; **Supervision**: Hamadjam Abboubakar and Henri Paul Ekobena Fouda; **Project administration**: Hamadjam Abboubakar and Henri Paul Ekobena Fouda; All authors have read and agreed to the published version of the manuscript.

Conflict of Interest

The authors declare that they have no conflicts of interest.

Funding

The authors did not receive support from any organization for the submitted work.

Ethical Conduct

Not applicable.

AI compliance

The authors declare that they have not used Artificial Intelligence (AI) tools in the creation of this article.

Data availability

The sources of data used in this work are mentioned in the text.

References

[1] A P Lemos-Paiao. C J Silva and D F M Torres. An epidemic model for cholera with optimal control treatment. *J. Comput. Appl. Math. 318*, page 168–180, (2017). doi: 10.1016/j.cam.2016.11.002. URL http://dx.doi.org/10.1016/j.cam.2016.11.002.

[2] World Health Organisation (WHO). Choléra, Accessed March 10, 2023. URL http://https://www.who.int/fr/news-room/fact-sheets/detail/cholera.

[3] Azman A S. Rudolph K E. Cummings D A. Lessler J. The incubation period of cholera: a systematic review. *J Infect*, 66;(5):432–8, 2013. doi: 10.1016/j.jinf.2012.11.013. URL https://www.ncbi.nlm.nih.gov/pubmed/23201968.

[4] Ali Mohammad. Nelson Allyson R. Lopez Anna Lena. Sack David A. Updated global burden of cholera in endemic countries. *PLOS Neglected Tropical Diseases*, 9(6):1–13, 06 2015. doi: 10.1371/journal.pntd.0003832. URL https://doi.org/10.1371/journal.pntd.0003832.

[5] World Health Organisation (WHO). Yemen: Weekly cholera bulletins, Accessed March 10, 2023. URL https://data.humdata.org/dataset/yemen-cholera-outbreak-daily-epidemiology-update.

[6] David Arnold. Cholera and colonialism in british india. *Past & Present*, 113:118–151, 1986.

[7] Srabani Sen. Indian cholera: a myth. *Indian Journal of History of Science*, 47(3):345–374, 2012.

[8] World Health Organisation (WHO). The telegraph news: Race against time to curb cholera outbreak in yemen, Accessed March 11, 2023. URL Availablefrom:https://www.telegraph.co.uk/news/0/race-against-time-curb-cholera-outbreak-yemen/.

[9] Radio France International (RFI). Archives monde du jeudi 20 avril 2023, 2023. URL https://www.rfi.fr/fr/archives/monde/2023/04/20-avril-2023.

[10] Podlubny I. Fractional differential equations. *Academic Press, San Diego*, 1998.

[11] R Fandio. H Abboubakar. H P Ekobena Fouda. A Kumar. K Sooppy Nisar. Mathematical modelling and projection of buruli ulcer transmission dynamics using classical and fractional derivatives: A case study of cameroon. *Partial Differential Equations in Applied Mathematics*, 2023. URL https://api.semanticscholar.org/CorpusID:265409890.

[12] Rashid Jan, Salah Boulaaras, Asma Alharbi, and Normy Norfiza Abdul Razak. Fractional-calculus analysis of the dynamics of a vector-borne infection with preventive measures. *Fractal & Fractional*, 8(12), 2024.

[13] Rashid Jan, Mansoor Alsulami, and Normy Norfiza Abdul Razak. Modeling the response of the immune system to hiv-tumor interaction via a fractional framework. *European Journal of Pure and Applied Mathematics*, 18(1):5670–5670, 2025.

[14] Vincenzo Capasso and Stefano L Paveri-Fontana. A mathematical model for the 1973 cholera epidemic in the european mediterranean region. *Revue d'epidemiologie et de sante publique*, 27 2:121–32, 1979.

[15] F. Ozkose. R Habbireeh. M T Senel. A novel fractional order modelof sars-cov-2 and cholera disease with real data. *Journal of Computational and AppliedMathematics*, (2022). doi: https://doi.org/10.1016/j.cam.2022.114969.

[16] Jin-Qiang Zha. Ebenezer Bonyah. Bing Yan. Muhammad Altaf Khan. K O Okosun. Mohammad Y Alshahrani. Taseer Muhammad. A mathematical model for the coinfection of buruli ulcer and cholera. *Results in Physics*, 29:2211–3797, 2021. doi: doi.org/10.1016/j.rinp.2021.104746. URL https://www.sciencedirect.com/science/article/pii/S2211379721008123.

[17] Abboubakar H. Fandio R. Sofack S B. and Ekobena Fouda H P. Fractional dynamics of a measles epidemic model. *Axioms*, 11(8):363, 2022. doi: doi.org/10.3390/axioms11080363.

[18] Abboubakar H. Raissa K. Fandio R. and Ekobena Fouda H P. Fractional modeling of hansen's disease (leprosy) transmission dynamics. *Colloque Africain sur la Recherche en Informatique et en Mathématiques Appliquées (CARI)*, hal-03702649, Oct 2022, Tunis, Tunisia. doi: HALId:hal-03702649. URL https://hal.archives-ouvertes.fr/hal-03702649.

[19] A P Lemos-Paiao. C J Silva and D F M Torres. A cholera mathematical model with vaccination and the biggest outbreak ofworld's history. *AIMS Mathematics*, 3(4):448–463, 2018. doi: DOI:10.3934/Math.2018.4.448. URL http://www.aimspress.com/journal/Math.

[20] Codeco Cláudia Torres. Endemic and epidemic dynamics of cholera: the role of the aquatic reservoir. *BMC Infectious Diseases*, 1(1):1471–2334, 2001. ISSN 1. doi: 10.1186/1471-2334-1-1. URL https://doi.org/10.1186/1471-2334-1-1.

[21] Hartley D M. Morris J G. and Smith D L. Hyperinfectivity : A critical element in the ability of v. cholerae to cause epidemics ? *PLoS Medicine*, 3(1):63–69, January 2006. ISSN 1549-1277. doi: 10.1371/journal.pmed.0030007.

[22] Mukandavire Z. Shu Liao, Jin Wang. Holly D Gaff. David L Smith., and J Glenn Morris. Estimating the reproductive numbers for the 2008–2009 cholera outbreaks in zimbabwe. *Proceedings of the National Academy of Sciences*, 108:8767 – 8772, 2011.

[23] Xu Chen. Jie Sheng. Xiaojun Wang. Jiangshan Deng. Exploring determinants of attraction and helpfulness of online product review: A consumer behaviour perspective. *Discrete Dynamics in Nature and Society*, 2016, 2016. ISSN 1026-0226. doi: 10.1155/2016/9354519. Publisher Copyright: © 2016 Xu Chen et al.

[24] E A Bakare. S Hoskova-Mayerova. Optimal control analysis of cholera dynamics in the presence of asymptotic transmission. *Axioms*, 10:60, 2021. URL https://api.semanticscholar.org/CorpusID:234824827.

[25] F Monje. A R Ario. A Musewa. K. Bainomugisha. B Basuta Mirembe. D M Aliddeki. D Eurien. G Nsereko. C Nanziri. E Kisaakye. V Ntono. B Kwesiga. D Kadobera. L Bulage. G Bwire. P Tusiime. Julie R Harris. Bao-Ping Zhu. A prolonged cholera outbreak caused by drinking contaminated stream water, kyangwali refugee settlement, hoima district, western uganda: 2018. *Infectious Diseases of Poverty*, 9, 2020. URL https://api.semanticscholar.org/CorpusID:226240276.

[26] Subchan. Irma Fitria. and Ahmad M Syafi'i. An epidemic cholera model with control treatment and

intervention. *Journal of Physics: Conference Series*, 1218(1):012046, may 2019. doi: 10.1088/1742-6596/1218/1/012046. URL https://dx.doi.org/10.1088/1742-6596/1218/1/012046.

[27] Mittag-Leffler G M. Sur la nouvelle fonction e(x). *Comptes Rendus de l'Académie des Sciences*, 137:554–558, 1903.

[28] Abdul Latif. *Banach Contraction Principle and Its Generalizations*. Springer Nature, 09 2014. ISBN 978-3-319-01585-9. doi: 10.1007/978-3-319-01586-6__2.

[29] Pauline van den Driessche. Reproduction numbers of infectious disease models. *Infectious Disease Modelling*, 2:288–303, 2017. doi: http://dx.doi.org/10.1016/j.idm.2017.06.002.

[30] Brouwer A F. Why the spectral radius ? an intuition-building introduction to the basic reproduction number. *Bulletin of Mathematical Biology*, 84:96, 2022. doi: https://doi.org/10.1007/s11538-022-01057-9.

[31] Abboubakar Hamadjam, Kom Regonne Raïssa, and Kottakkaran Nisar. Fractional dynamics of typhoid fever transmission models with mass vaccination perspectives. *Fractal and Fractional*, 5:149, 09 2021. doi: 10.3390/fractalfract5040149.

[32] Hamadjam Abboubakar, Lausaire Kemayou Kombou, Adamou Dang Koko, Henri Paul Ekobena Fouda, and Anoop Kumar. Projections and fractional dynamics of the typhoid fever: A case study of mbandjock in the centre region of cameroon. *Chaos Solitons & Fractals*, Vol. 150:p. 111–129, 2021. doi: https://doi.org/10.1016/j.chaos.2021.111129.

[33] Shuai Z. van den Driessche P. Global stability of infectious disease models using lyapunov functions. *SIAM Journal on Applied Mathematics*, 73:1513–1532, 2013. doi: https://doi.org/10.1137/120876642.

[34] J.P. La Salle. The stability of dynamical systems. *SIAM, Philadelphia*, vol. 25, 1976.

[35] Hamadjam Abboubakar. Pushpendra Kumar. Norodin A Rangaig. Sachin Kumar. A malaria model with caputo–fabrizioand atangana–baleanu derivatives. *International Journal of Modeling, Simulation, and Scientific Computing*, 2150013, 2021. doi: DOI:10.1142/S1793962321500136.

[36] Al Karim Datoo. Shakeel Ahmed. Insaf Ali. Comparative analysis of non-formal educational strategies for out-of-school children (oosc) in bhutan, india, and pakistan: Transferring insights for pakistan. *Pakistan Journal of Educational Research*, 7(3):246–266, 2024. doi: https://doi.org/10.52337/pjer.v7i3.1169.

[37] G. Vijayalakshmi and M. Ariyanatchi. Adams–bashforth moulton numerical approach on dengue fractional atangana baleanu caputo model and stability analysis. *International Journal of Applied and Computational Mathematics*, 10, 01 2024. doi: 10.1007/s40819-023-01652-x.

[38] Kai Diethelm and Neville J. Ford. Analysis of fractional differential equations. *Journal of Mathematical Analysis and Applications*, 265(2):229–248, 2002. ISSN 0022-247X. doi: https://doi.org/10.1006/jmaa.2000.7194. URL https://www.sciencedirect.com/science/article/pii/S0022247X00971944.

[39] Kai Diethelm. An algorithm for the numerical solution of differential equations of fractional order. *Electronic Transactions on Numerical Analysis*, 5, 08 1998.

[40] Baskonus Haci Mehmet and Bulut Hasan. On the numerical solutions of some fractional ordinary differential equations by fractional adams-bashforth-moulton method. *Open Mathematics*, vol. 13, no. 1:pp. 547–556, 2015. doi: https://doi.org/10.1515/math-2015-0052.

[41] Ayesha Sohail. Khadija Maqbool. Rahmat Ellahi. Stability analysis for fractional-order partial differential equations by means of space spectral time adams-bashforth moulton method. *Numerical Methods for Partial Differential Equations*, 34(1):p. 19–29, 2017. doi: DOI10.1002/num.22171.

[42] Chitnis N. Hyman J M. Cushing J M. Determining important parameters in the spread of malaria through the sensitivity analysis of a mathematical model. *Bulletin of Mathematical Biology*, 70:1272–1296, 2008. doi: https://doi.org/10.1007/s11538-008-9299-0.